Nigerian Research Journal of Engineering and Environmental Sciences 9(1) 2024 pp. 362-395
p ISSN: 2635-3342; e ISSN: 2635-3350

Nigerian Research Journal of Engineering and Environmental Sciences
Journal homepage: www.rjees.com

Original Research Article

Adsorption Kinetics of Congo Red Dye Using Acid Modified Umuahia Clay: Modeling and Optimization Analysis

***[1]Oguanobi, N.C., [1]Ude, C.N., [2]Onukwuli, O.D., [1]Anike, E.N. and [1]Kalu, C.B.**

[1]Department of Chemical Engineering, Michael Okpara University of Agriculture, PMB 7267, Umudike, Abia State, Nigeria.
[2]Department of Chemical Engineering, Nnamdi Azikiwe University, PMB 5025, Awka, Nigeria.
*oguanobi.nonso@mouau.edu.ng

http://doi.org/10.5281/zenodo.12599888

ARTICLE INFORMATION

Article history:
Received 05 May. 2024
Revised 08 Jun. 2024
Accepted 13 Jun. 2024
Available online 30 Jun. 2024

Keywords:
Adsorption
Isotherm
Optimization
Thermodynamics
Fourier transform infrared

ABSTRACT

Congo red dye (CR) effluent is a toxic waste of environmental concern due to its artificial origin and complex molecular structure, which make it non-biodegradable. This research focused on using the physical method to remove CR pollutants (color, dissolved salt (EC), total dissolved solids (TDS), and chemical oxygen demand (COD)) from aqueous solutions by investigating the adsorptive qualities of acid-modified Umuahia clay (AUC). The batch system was applied to evaluate the effect of process-independent variables on the adsorption process. The mechanism of adsorption was investigated using intra-particle diffusion, liquid film, and the Boyd model. The thermodynamic properties ΔS, ΔH, ΔG, and Ea were determined. The optimum removal efficiency of CR was predicted using the artificial neural networks (ANN), adaptive neuro-fuzzy inference systems (ANFIS), and response surface methodology (RSM) models. The activation resulted in an increase in surface area. Maximum color removal of 99.99% was observed at pH 2, adsorbent dosage of 0.5 g, adsorbent particle size of 50 µm, initial dye concentration of 100 mg/l, contact time of 130 min, and a temperature of 333 K. A maximum adsorption capacity of 140.53 mg/g was obtained. The adsorption mechanism was influenced by multiple steps. Thermodynamic results suggested an endothermic, favorable, spontaneous, and physical adsorption process. The ANFIS model, with an R^2 of 0.9999, is statistically more significant than the ANN and RSM models. A maximum reusability capacity of 97.2% was achieved after three cycles. The obtained results confirm AUC as a reliable, cost-effective alternative adsorbent for CR removal from effluents.

1. INTRODUCTION

Water pollution has been a great trait in both developed and developing countries due to the revolution in society from a pre-industrial-based economy to an industrial economy. The transition in the economy has

positively benefited mankind but negatively impacted the aquatic and terrestrial environments, if not the ecosystem at large. This adverse effect of the transition in the economy is linked to a series of pollutants from different industries, especially the oil refining industries, which generate wastewater containing oil and dissolved substances, and the dye production and consumption industries, which generate wastewater containing color, suspended solids, chemical oxygen demand, biochemical oxygen demand, and perilous chemicals (heavy metals) in great quantities (Oguanobi et al., 2024b) Among the many sources of industrial dye wastewater are textile, rubber, leather, paper and pulp, plastic, soap and detergent, food, paint, petrochemical, photographic, printing ink, pharmaceutical, cosmetics, mills, and mining operations (Oguanobi et al., 2024a). The high rate of water pollution is linked to poor waste management, which is a result of a lack of technical know-how and a lack of strict laws regulating the discharge of sewage or inadequately treated effluents into the environment (Oguanobi et al., 2024b). Recently, different physical and chemical treatment techniques such as coagulation and flocculation, sonochemical degradation, adsorption, photochemical degradation, electrochemical removal, electrochemical degradation, membrane separation, bio-degradation, fento-biological treatment scheme, photo-fento process, and oxidation and zonation have been explored in trying to eradicate the trait of water pollution from the source (Oguanobi *et al.,* 2024a).. All of these techniques, with the exception of adsorption, have some drawbacks, and none of them have been able to totally eliminate color from wastewater (Oguanobi *et al.* 2019).

Adsorption is a unit operation and a mass transfer operation process that involves the adhesion of molecules, ions, and atoms from a liquid, dissolved solid, or gas to the surface of a material called an adsorbent. Therefore, an adsorbent is any material that is capable of removing from an aqueous solution dissolved components through the force of attraction that exits between the aqueous solution (adsorbate) and the surface of the adsorbent. This unit operation process finds great use in many industrial applications where water recovery is essential, such as textile, rubber, leather, paper and pulp, plastic, soap and detergent, food, paint, petrochemical, photographic, printing ink, pharmaceuticals, cosmetics, etc. Activated carbon has been the conventional adsorbent for the adsorption process over time due to its uniqueness and high adsorption capacity, but the limitation of high operating costs becomes a serious concern and thereby raises the quest for a non-conventional, low-cost alternative. Different non-conventional adsorbents have been exploited, and all show the capacity to replace conventional activated carbon. Some of the previously exploited non-conventional adsorbents include modified clays (Oguanobi et al., 2019, Nayoon et al, 2022), hazelnut shell (Do˘gan et al., 2009), modified biomass (Mohammed et al., 2023), red Clay (Muhammed and Çiğdem, 2022), Eggplant biomass (Zhi et al., 2022), black stone cherries (Arana and Mazzoco 2010) agriculture waste (Dal and Meenal, 2022) neem leaf powder (Bhattacharyya and Sharma, 2005), rice hull (El-Halwany, 2010), rice bran (Mojtaba et al. 2020), and rice husk (Onu et al., 2020), clay mineral (Mohammed et al., 2022; Juraj, 2023; and Zineb et al., 2023,) zeolite-based bio membrane (Sabarish et al., 2022), among others. However, among all these exploited adsorbents, clays exhibit high adsorption capacity due to their ability to adsorb ions and molecules on both external and interlayer particle sites.

Adsorption and desorption of organic molecules in clays are basically controlled by the surface properties of the clay, such as its large surface area, low permeability, high retention, and cation exchange capacities. Natural clay exhibits a negative charge of structure, which allows it to adsorb positively charged dyes but induces a low adsorption capacity for anionic dyes (Mahammedi and Benguella, 2016). The natural high adsorption strengths of clay can be further enhanced through modification. Modification of clay creates positive charged structure which also allows the adsorption of anionic dyes (negatively charged dye). Most works on CR dye removal have focused on studying the influence of these factors using the one factor at a time method, which is cumbersome, time-consuming, and cannot satisfactorily predict the optimum point of process variables.

RSM is a model used to generate a mathematical model that can satisfactorily give the optimum parameters for operating a process. It helps in the simultaneous examination of process variables that affect a process, even in the presence of complex interactions. RSM only needs small experimental runs to predict an optimum condition. ANN uses artificial neurons to process information. It is used to evaluate complex nonlinear problems with sizable data sets. It also analyzes problematic data sets that are difficult to tackle ordinarily.

ANFIS is a kind of artificial intelligence model or concept that utilizes the learnings of fuzzy logic and neural networks to generate a hybrid model that yields an effective and precise result. ANFIS is applicable to both linear and nonlinear systems with a great level of accuracy. It is also a kind of ANN that is based on a Takagi-Sugeno fuzzy inference system (Gonzalez et al., 2020).

The objective of this work was to study the effect of acid activation on the adsorptive properties of Umuahia clays on the removal of pollutants from Congo red dyes from an aqueous solution. It also utilizes artificial intelligent optimization models such as response surface methodology (RSM), artificial neural networks (ANN), and adaptive neuro-fuzzy inference systems (ANFIS) in modeling and predicting the optimum removal of CR dye from wastewater.

2. MATERIALS AND METHODS

2.1. Materials

The primary raw material used is pure white-colored clay obtained from Umudike village in Umuahia south Local Government Area of Abia state Nigeria, while the secondary raw materials used were all of analytical grade. All the solutions used were prepared with distilled water.

2.2. Acid Activation of Clay Sample

The clay material for activation was sun dried for three days and reduced to mesh size with Laboratory mortar and pestle. The mesh clay sample was sieved using 50 µm particle size dry test sieves. The sieved clay sample was mixed with H_2SO_4 in a conical flask in w/v ratio of 1:6 (200 g of meshed clay sample was dissolved with 1200 ml of the prepared acid) and allowed for 24 hours. The slurry was filtered at the expiration of 24 hours to separate the clay and the acid. The obtained clay residue was washed with distilled water until a neutral pH point was reached with pH indicator. The neutral clay slurry was dried with an oven temperature of 80 ^oC for 240 seconds (4 hours). The obtained dried activated sample was crushed, sieved using 50 µm particle size dry test sieves and stored in a desiccator until used. This acid activation method used align with the method used in previous research conducted by Oguanobi et al. (2019, 2024a).

2.3. Characterization

The activated and raw clay sample was analyzed to determine the functional group present and observe surface morphologies. The functional group analysis is as well called Fourier transform infrared (FTIR) analysis and it was carried out using Shimadzu spectrophotometer model S8400, with samples prepared by conventional KBr disc method. The surface morphology analysis is as well called Scanning Electron Microscope (SEM) analysis and it was carried out using Joel scanning electron microscope model JSM 6400 with coated gold film of layers approximately 20-25 A thick.

2.4. Batch Adsorption Studies

Batch adsorption studies were conducted to investigate the process parametric effects of adsorbent particle size, adsorbent dose, initial adsorbate concentration, adsorption time, pH and temperature for CR uptake on modified clay adsorbent. CR solution was prepared by dissolving a known quantity of dye crystal in distilled water. The solution obtained was used as a stock solution and diluted to the required initial concentration range of 100 to 300 mg L^{-1}. The adjustment of pH of the solution was achieved by using either 0.1 N HCl or NaOH. The resulted effect of studied process variables on CR uptake were determined using of UV-visible spectrophotometer for color removal, conductivity meter for total dissolved solid (TDS) and electrical conductivity (EC) removal, and chemical oxygen demand analyzer for chemical oxygen demand (COD) removal.

2.5. Equilibrium/Isotherm Studies

Equilibrium adsorption experiment was carried out by contacting a fixed quantity of adsorbent into glass beakers (200 ml) containing a definite volume of different concentrations of CR dye solution of the same pH level. These beakers containing the mixture/solute were placed on shaker (magnetic stirrers) regulated at

the fixed temperature level for a period of 130 minutes to ensure equilibrium was reached. The equilibrium concentration of dye is determined using UV-visible spectrophotometer.

At equilibrium, dye uptake "qe" (mg g^{-1}), was evaluated using expression of Equation 1.

$$qe = \frac{(C_o - c_e)V}{m} \quad (1)$$

Percentage dye uptake was evaluated using Equation 2.

$$\% \text{ Adsorption} = \frac{(C_o - c_e)}{C_o} \times 100 \quad (2)$$

Where C_o and C_e(mg L^{-1}) were initial and equilibrium dye concentrations respectively, while V and m were the volume of the solution in liter and the mass of dry sorbent used in gram.

Adsorption isotherm is of paramount important in any adsorption system to describe the relationship between the adsorbate and adsorbent. In this research work six isotherm models were employed: the Langmuir (Langmuir, 1916), the Freundlich (Freundlich 1906), the Vieth–Sladek (Vieth and Sladek, 1965), and the Dubinin–Redushkevich (Dubinin and Redushkevich, 1947), the Redlich-Peterson (Redlich-Peterson, 1959), and the Jovanovic (Jovanovic, 1969) with their expressions (non-linearized forms) listed in equation no 3-8. The parameters of each model provide vital information on the adsorption mechanisms, surface properties and adsorbent affinity.

2.5.1. Langmuir adsorption isotherm

Langmuir isotherm expression describes adsorption homogeneity (homogeneous adsorption) as a process where all active sites have even energies and indistinguishable affinity for adsorbate onto the surface without the migration of molecules between localized surfaces. The non-linearized form of the Langmuir model can be expressed as follows:

$$q_e = \frac{Q_m K_L C_e}{1 + K_L C_e} \quad (3a)$$

Where q_m (mg/g) is Langmuir adsorption capacity constants, K_L (L/mg) is Langmuir energy/affinity of adsorption constants, C_e (mg/L) is the equilibrium concentration, q_e (mg g^{-1}) is the amount of dye adsorbed at equilibrium

When the K_L value is high (greater than 1), it indicates that the adsorbate molecules have a high affinity for the adsorbent surface (strong adsorption). A K_L value of unity (K_L = 1) implies that the adsorption process is at equilibrium, with no significant preference for adsorption or desorption. When K_L is greater than zero but less than unity (0 < KL < 1), it indicates that the gas molecules have low affinity for the adsorbent (weak adsorption). Finally, a K_L value of zero (K_L = 0) implies that there is no interaction between the adsorbate and the adsorbent (no adsorption).

The essential feature of the Langmuir isotherm was expressed by means of R_L, a dimensionless constant referred to as the separation factor or equilibrium parameter. R_L is calculated using expression of Equation 3b.

$$R_L = \frac{1}{1 + K_L C_o} \quad (3b)$$

The value of R_L classifies the adsorption process into the following categories: unfavorable (R_L >1), linear (R_L =1), favorable (0<R_L<1), or irreversible (R_L=0).

2.5.2. Freundlich adsorption isotherm

The Freundlich model presumes that the adsorption process occurs on heterogeneous solid surfaces (non-uniform surfaces with a varying range of adsorption energies). The Freundlich adsorption isotherm is a two-

parameter isotherm that explains the relationship between the pressure or concentration of the adsorbate at a constant temperature and the quantity of adsorbate adsorbed onto an adsorbent (a solid surface). The non-linearized form of the Freundlich model can be expressed as follows:

$$q_e = K_F C_e^{\ 1/n_F} \tag{4}$$

Where C_e (mg/L) is the equilibrium concentration, q_e (mg g^{-1}) is the amount of dye adsorbed at equilibrium, K_F is Freundlich adsorption capacity and affinity constants and n is the Freundlich adsorption intensity and mechanism constants, $1/n_f$ is a measure of the surface heterogeneity of the adsorption site.

When the n value is close to unity (1), it signifies that the adsorption sites have uniform energies, thereby suggesting a more homogeneous solid surface. This outcome certifies that the adsorption process will be better suited to BET or Langmuir isotherms. When the n value is "n < 1 or n > 1," it indicates that adsorption sites have non-uniform energies, which makes the surface more heterogeneous. This outcome certifies that the adsorption process will be best described by the Freundlich isotherm model, which is better suited to heterogeneous surfaces (adsorbents with varying adsorption energies across the surface). The n_f value within the range of $1<n_f<10$, indicates a favorable and physical adsorption whereas and any value outside the range of $1<n_f<10$ suggests a linear and chemical process. When the K_F value is high, it indicates a greater affinity of the adsorbate for the adsorbent, which leads to a higher adsorption capacity of the adsorbent, whereas a smaller value of K_F suggests a weaker affinity of the adsorbate for the adsorbent, resulting in poor adsorption capacity.

2.5.3. Dubinin-Radushkevich adsorption isotherm

The Dubinin-Radushkevich isotherm model postulates that adsorption occurs due to the formation of indistinguishable energy wells within the porous structure of the adsorbent. These wells are formed by the interactions between the adsorbate molecules and the adsorbent. Additionally, this empirical model is used to represent the adsorption mechanism on surfaces with variability in adsorption energies using a Gaussian distribution of photon energy. The DR isotherm also estimates the maximum adsorption capacity (Q_m) of the adsorbent, which is an important parameter for evaluating the performance of an adsorbent. The non-linearized form of the Dubinin-Radushkevich model can be expressed as follows:

$$q_e = Q_m \exp\left(-b_{DR}\left[RT\, ln\left(1+\frac{1}{C_e}\right)\right]^2\right) \tag{5a}$$

Where Q_m (mg/g) is the maximum adsorption capacity constants, C_e (mg/L) is the equilibrium concentration, q_e (mg g^{-1}) is the amount of dye adsorbed at equilibrium. b_{DR} is a constant related to the adsorbent's structural characteristics and the energy distribution of the adsorption sites.

The adsorption mechanism is being examined through the mean free energy "E" value obtained from D-R model. The D-R model constant b_{DR} relates to the mean free energy of adsorption through the expression of Equation 5b.

$$E = \frac{1}{\sqrt{2b_{DR}}} \tag{5b}$$

When the b_{DR} value is small, it suggests a narrow energy distribution and probably a possible homogeneous system, whereas a larger value of b_{DR} indicates a broader energy distribution and a possible heterogeneous system.

2.5.4. Vieth-Sladek adsorption isotherm

The Vieth-Sladek isotherm is an extension of the Langmuir adsorption isotherm but incorporates a second term that account for the interaction between adsorbed molecules. This empirical model describes the adsorption process in terms of both multilayer and monolayer adsorption. In multilayer adsorption, adsorbate molecules adsorb onto the solid surface forms multiple layers on top of each other, unlike the D-R model,

which focus only on localized energy wells within the porous structure. The Vieth-Sladek isotherm also provide information on adsorbent maximum adsorption capacity (qm), which is an important parameter for evaluating adsorbent performance. Additionally, this model presumes that the adsorption process is governed by the competition between the attractive forces between the solid surfaces and the gas molecules and the repulsive forces between the gas molecules themselves. The non-linearized form of the Vieth-Sladek model can be expressed as follows:

$$q_e = K_{vs}C_e + \frac{Q_m B_{vs} C_e}{1 + B_{vs}C_e} \tag{6}$$

Where Q_m (mg/g) is Vieth–Sladek adsorption capacity constants, C_e (mg/L) is the equilibrium concentration, q_e (mg g^{-1}) is the amount of dye adsorbed at equilibrium, k_{vs} is the rate constant for the adsorption reaction, which depends on temperature (it describes the adsorption process's affinity for the adsorbent), and B_{vs} is Vieth–Sladek constants related to the rate of the adsorption and desorption reactions (it describes the adsorption process's behavior and the interaction between adsorbed molecules).

A high value of k_{vs} signifies that the adsorbent has a strong affinity for the gas molecule, whereas a low value indicates weak interaction. A high value of B_{vs} suggests strong interaction between adsorbed molecules, whereas a low value indicates poor interaction.

2.5.5. Redlich–Peterson isotherm

The Redlich-Peterson isotherm model is a three-parameter isotherm. The model design equation incorporates the feature of Freundlich and Langmuir, which signifies that it describes the adsorption on both heterogeneous and homogeneous surfaces. Redlich-Peterson invents this empirical equation to shed more light on the adsorption behavior of real systems, which deviate from the simplified presumptions made individually by the Freundlich and Langmuir isotherms.

The non-linearized form of the Redlich–Peterson model can be expressed as follows:

$$q_e = \frac{K_R C_e}{1 + a_R {C_e}^g} \tag{7}$$

Where C_e (mg/L) is the equilibrium concentration, q_e (mg g^{-1}) is the amount of dye adsorbed at equilibrium, K_R (L/g) is constant related to the adsorption capacity and affinity of the adsorbent, a_R (L mg^{-1}) is constant related to the adsorption capacity, and g (dimensionless) are the Redlich–Paterson constant. The values of g fluctuate between 0 and 1. A low g value (g tends to zero) suggest heterogeneous adsorption characteristics of Freundlich isotherm (Henry's law), while high g value very close to unity signify homogeneous or monolayer adsorption characteristic of Langmuir isotherm. Additionally, the g value helps to interpret the extent to which a gas deviates from ideal gas behavior, with higher values suggesting closer adherence to ideal gas behavior and lower values suggesting more significant deviations due to stronger intermolecular forces.

When the a_R value is high, it indicates the adsorbent has a good ability to adsorb and retain more adsorbate molecules at a given temperature, whereas a low value signifies poor adsorption and retaining ability of the adsorbent. When the K_R value is high, it indicates the adsorbent has a great adsorption capacity and affinity for the adsorbate, whereas a low value signifies poor adsorbent adsorption capacity and affinity for the adsorbate.

2.5.6. Jovanovic adsorption isotherm

The Jovanovic isotherm model is a two-parameter isotherm designed based on the assumptions of the Langmuir isotherm model but assumes surface adsorption and zero correlation between molecules. This empirical model permits some mechanical contact between the adsorbent and the adsorbate and accepts surface vibration of an adsorbed species. It can also be used for adsorption with both mobile and confined monolayers without lateral contact, however it is less effective in physical adsorption due to the adjustment

of the adsorption surface from this model. Furthermore, the Jovanovic isotherm model equation simplifies to Freundlich isotherm (Henry's law) at low concentrations and can reach the saturation limit at high concentrations. The non-linearized form of the Jovanovic model can be expressed as follows:

$$q_e = Q_m(1 - exp^{-K_J C_e}) \quad (8)$$

Where q_m (mg/g) is Jovanovic adsorption capacity constants, C_e (mg/L) is the equilibrium concentration, q_e (mg g^{-1}) is the amount of dye adsorbed at equilibrium. K_J (L mg^{-1}) is the equilibrium constant of Jovanovic isotherm and it represents the adsorption affinity of the adsorbate for the adsorbent. It also helps to determine the extent of adsorption at different concentrations.

2.6. Kinetic Studies

In kinetic experiments, aqueous samples were taken at different time intervals to determine the uptake of dye at any preset time t.

At time t, dye uptake "qt" (mg g^{-1}) was evaluated using Equation 9.

$$qt = \frac{(C_o - C_t)V}{m} \quad (9)$$

Where C_t is dye concentration at any time t.

2.6.1. Pseudo-first-order model

The pseudo-first-order kinetic postulates that the rate of the reaction appears to depend on the concentration of one reactant, but in reality, it may involve other factors as well. The non-linearized form of the pseudo-first-order model can be expressed as follows:

$$q_t = q_e[1 - exp(K_1 t)] \quad (10)$$

Where q_e (mg/g) is the amount of adsorbate adsorbed at equilibrium, q_t (mg/g) is the amount of adsorbate adsorbed at time t. K_1 (min^{-1}) is the adsorption rate constants for pseudo-first-order.

2.6.2. Pseudo-second-order model

The pseudo-second-order kinetic theory postulates that the concentration of the adsorbate and the product of the remaining accessible adsorption sites determine the rate of reaction, so the kinetic model is an empirical model used to analyze the reaction kinetics of different chemical processes. The non-linearized form of the pseudo-first-order model can be expressed as follows:

$$q_t = \frac{K_2 q_e^2 t}{1 + K_2 q_e t} \quad (11)$$

Where q_e (mg/g) is the amount of adsorbate adsorbed at equilibrium, q_t (mg/g) is the amount of adsorbate adsorbed at time t, K_2 gmg^{-1}min were the adsorption rate constants pseudo-second-order.

2.6.3. Elovich model

The Elovich kinetic theory postulates that the adsorbent surfaces are energetically heterogeneous. This model presumes that the adsorption kinetics will not be affected by interactions between the adsorbed and desorption ions, even at low surface coverage. The major effect of energetic heterogeneity surfaces on sorption equilibrium in gas-solid systems has been proven, while that of liquid-solid systems is yet to be established. The non-linearized form of the pseudo-first-order model can be expressed as follows:

$$q_t = \frac{1}{\beta}\ln(1 + \alpha\beta t) \quad (12)$$

Where q_t (mg/g) is the amount of adsorbate adsorbed at time t, α is the Elovich constant for the initial adsorption rate, and β is the Elovich desorption constant.

When the value of α is high, it suggests a faster initial adsorption rate, meaning that the adsorbent has a high affinity for the gas molecule, whereas a smaller value of α indicates a slow initial adsorption rate. A higher value of β suggests high adsorption capacity, which means that the adsorbent surface cannot easily desorbed the adsorbate molecules, whereas a small value of β indicates easily reversible process.

2.6.4. Pseudo-nth order

The pseudo-nth-order kinetic model is an empirical model used to analyze chemical systems where the reaction order is not naturally an integer, and it's an extension of the first- and second-order kinetic models. The model can be applied to different types of reactions, which include heterogeneous and homogeneous reactions. The non-linearized form of the pseudo-first-order model can be expressed as follows:

$$q_t = q_e - [q_e^{1-n} - (1-n)K_n t]^{1/(1-n)} \quad (13)$$

Where q_e (mg/g) is the amount of adsorbate adsorbed at equilibrium, q_t (mg/g) is the amount of adsorbate adsorbed at time t. K_n ($gmg^{-1}min$) were the adsorption rate constants for pseudo-nth-order; n is the order of reaction.

When the value of n is high (n > 1), it indicates that the rate of reaction of the reactant concentration is likely to change, whereas a smaller value of n (0 < n < 1) suggests that the reaction rate of the reactant concentration is unlikely to change. A value of n = 1 represents a first-order reaction, while n = 0 represents a zero-order reaction. A high k value suggests a faster reaction rate, whereas a smaller value indicates a slower reaction rate. The rate constant can be used to calculate the half-life of the reaction or the time required for the reaction progress variable (x) to reach a specific value.

2.6.5. Fractional power model

The fractional power kinetic model is a modified form of the Freundlich model. This empirical model calculates the exact rate of adsorption at a unit time using the model product's constant. The non-linearized form of the pseudo-first-order model can be expressed as follows:

$$q_t = Kt^V \quad (14)$$

Where q_t (mg/g) is the amount of adsorbate adsorbed at time t, this parameter "t" should not contain a value equal to zero to prevent infinite value. K(mg g-1) is the fractional power constant and v is the fractional power rate constant.

2.7. Adsorption Thermodynamics

Thermodynamics studies were to determine the energy changes involved in the adsorption. Thermodynamic parameters are calculated using the following equations

$$\Delta G^0 = \Delta H^0 - T\Delta S^0 \quad (15)$$

$$\Delta G^o = -RT \ln K_c \quad (16)$$

$$K_c = \frac{C_s}{C_e} \quad (17)$$

$$\ln K_c = \left(\frac{\Delta S}{R}\right) - \left(\frac{\Delta H}{RT}\right) \quad (18)$$

Where ΔG^o, ΔH, ΔS are the standard; Gibbs free energy change, enthalpy change (heat of reaction) and entropy change, respectively. $K_c$is the equilibrium constant, C_s is the equilibrium concentration of CR on solid (adsorbent (mg/L)), R is the general gas constant (8.314 J/mol/K) and T is adsorption temperature on Kelvin scale.

The nature of adsorption process can be inferred from the level of activation energy. The Arrhenius rate expression of equations 19 and 20 were used to evaluate the activation energy of adsorption.

$$K_A = Ae^{-Ea/RT} \tag{19}$$

$$InK_A = InA - \frac{Ea}{RT} \tag{20}$$

Where Ea is the Arrhenius activation energy (KJ/mol) K_A is a pseudo-second-order rate constant of adsorption (g/mg min), R is the universal gas constant (8.314J/molK) and T is the absolute solution temperature (k). Ea Can be calculated from the plot of InK_A versus 1/T.

2.8. RSM Modeling

Design expert version 13 was used in both the design and the RSM-CCD analysis. The experiment was designed using a central composite design (CCD) with five factor levels as shown below in Table 1. RSM uses data obtained from design of experiments and statistical modeling technique to solve multi-variant problems (Venkatesh and Karthikeyan 2018).

Table 1: Five factor levels of the independent variables

Process parameter	+α	+1	0	-1	-α
Temperature (°C)	64.1421	60.00	50.00	40.00	35.8579
Concentration (mg/l)	341.421	300.00	200.00	100.00	58.578
pH	11.6568	10.00	6.00	0.34316	52.07
Adsorbent dose (g)	0.582842	0.500	0.300	0.100	0.017158

The independent variables used were temperature, pH, concentration and dosage while the actual response (percentage adsorbed) was the dependent variable. The data set for RSM-CCD experiment can be evaluated using expression of Equation 21 (Arulkumar et al. 2011).

$$Q = 2^q + 2q + q_c \tag{21}$$

Where q is the number of input factors and 2^q, 2q and q_c represents the: factorial points, axial points, and center points. Furthermore, the total number of factorial and star points were tripled to maximize the dependability of the design and ten center points were used. As a result, a total of 82 experimental data sets were assessed. The experiment was conducted at random to eliminate systematic error. The link between the process variables and dependent variables was estimated using second-order polynomial as in equation 22.

$$R = \beta_o + \sum_{i=1}^{k} \beta_i \alpha_i \ldots\ldots + \ldots \sum_{i=1}^{k} \beta_{ii} \alpha_i^2 \ldots\ldots + \cdots \sum_{i=1}^{k-1} \sum_{j=1}^{k} \beta_{ij} \alpha_i \alpha_j \tag{22}$$

Where R is the calculated response, β_o is the model constant, β_i, β_{ii} and β_{ij} are the calculated coefficients second-order polynomial expression for the linear, quadratic and products of α_i, α_i^2 and $\alpha_i \alpha_j$, respectively.

2.9. ANN Modeling

Artificial neural networks (ANN) were used to model and analyze the percentage of CR dye adsorbed using the neural network toolbox of MATLAB R2021. The weighted inputs that arrive at each neuron in a biological system are processed through a nonlinear activation function to create an output signal (Manpreet et al., 2011). The data sets used in RSM-CCD analysis were tripled and used in the ANN for accurate modeling process. The validation, training, and testing data sets each received a randomly assigned percentage of 15%, 70%, and 15% of the total data sets. The ANN architecture comprises the input nodes, hidden neuron layers, and output nodes (Figure 1). To prevent over-fitting and a decrease in the convergence rate, the optimal number of hidden layers was established by iteration (Mingyi et al., 2017). The metrics were maximum correlation coefficient (R2) and minimum mean square error (MSE). The learning approach for the modeling was a Multi-Layer Perceptron (MPL) that used back propagation. The training function, trainlm, was utilized to regularize the bias value. To lessen network error, the process parameters and the response were standardized between 0 and 1 (Mourabet et al., 2014).

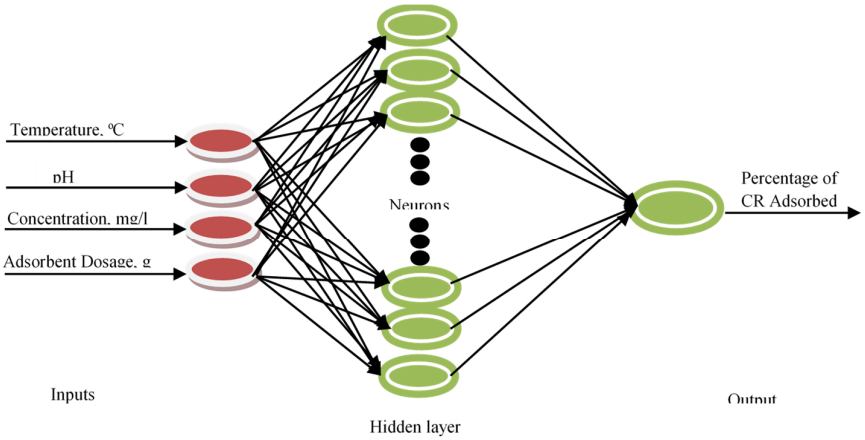

Figure 1: ANN architecture of CR removal

2.10. ANFIS Modeling

ANFIS model was used to model and predict the optimum CR dye adsorbed, through Mathworks Inc. R2021. The ANFIS is represented as a five-layered network using the fuzzy inference system (FIS) concept, as shown in Figure 2. Temperature, concentration, dosage, and pH are the process variables that the first layer of the fuzzy system network accepts as inputs. The fuzzy rules were chosen in the second layer node and passed on to the third layer so that the activity rules could be normalized.

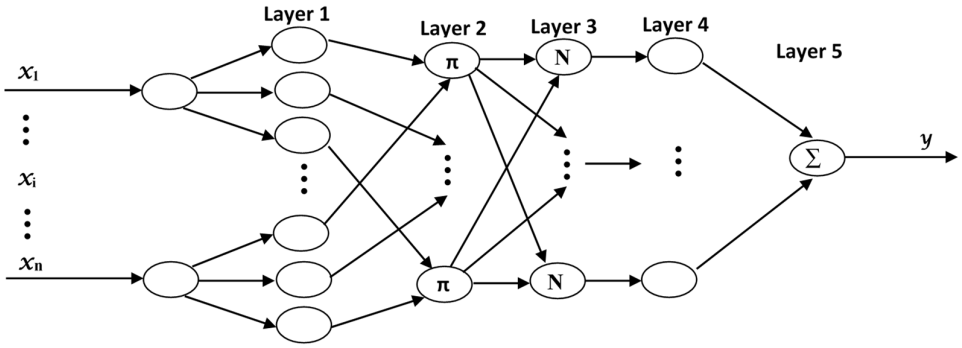

Figure 2: ANFIS structure

The fourth layer accepts the nodes, converges the parameters, and sends them as a single output layer (percentage of CR adsorbed) to the fifth layer (Bahman et al., 2018). The ANFIS modeling utilized the same set of data as the ANN modeling (two hundred and forty-six data sets). A hybrid optimization approach was applied with zero error tolerance.

2.11. Comparative Analysis of RSM, ANN, and ANFIS Models

The actual CR adsorption values were compared to the predicted adsorption values by RSM, ANN, and ANFIS and subjected to statistical error indices. Five out of the seven statistical error functions given in Table 2 were used for comparative analysis. The normalized standard deviation and Chi-square test error functions were statistical error tool used to determine the best-fit equilibrium and kinetic model for the system.

Table 2: Statistical error functions used

Error function	Equation	Equation number
Correlation coefficient	$R^2 = 1 - \frac{\sum_{i=1}^{N}(\mathrm{M_{exp}} - \mathrm{M_{pre}})^2}{\sum_{i=1}^{N}(\mathrm{M_{exp}} - M_m)^2}$	(23)
Average percentage error	$APE = \sum_{i-1}^{N} \frac{\left\|q_{e\,exp} - q_{e\,cal}/q_{e\,exp}\right\|}{N} X\ 100$	(24)
Sum of squared error	$\mathrm{SSE} = \sum_{\mathrm{i=1}}^{\mathrm{N}} \left(\mathrm{M_{exp}} - \mathrm{M_{pre}}\right)^2$	(25)
Root mean square error	$RMSE = \sqrt{\frac{1}{N-2}\sum_{i=1}^{N}\left(\mathrm{M_{exp}} - \mathrm{M_{pre}}\right)^2}$	(26)
Hybrid fractional error function	$HYBRD = \sum_{\mathrm{i=1}}^{\mathrm{N}} \frac{\left(\mathrm{M_{exp}} - \mathrm{M_{pre}}\right)^2}{\mathrm{M_{exp}}}$	(27)
Normalized standard deviation	$NSD = 100 \times \sqrt{\frac{\sum_{i}^{N}[(q_e\,\mathrm{exp} - q_e cal)/q_e exp]^2}{N-1}}$	(28)
Chi-square test	$x^2 = \sum_{N=1}^{N} \frac{(q_{e,exp} - q_{e,cal})^2}{q_{e,cal}}$	(29)

Where N is the number of experimental runs; $\mathrm{M_{exp}}$ is the experimental values for the modeling; $\mathrm{M_{pre}}$ is the model predicted value; $M_m$is the experimental mean value, $q_{e,exp}$ and $q_{e,cal}$ are the experimental values and model calculated values respectively

These error functions were used to investigate the accuracy of the models in predicting the removal of CR from aqueous solutions by the adsorption process. The significance of the sum of squared errors (SSE), average percentage error (APE), hybrid fractional error function (HYBRID), and root mean square error (RMSE) models was based on the fact that the smaller the values of the result, the better the system, while the correlation coefficient (R^2) is that the higher the value of the result to unity, the better the system.

2.12. Dissolve Salts and Solid Analysis

This analysis was carried out using a DDS-307A conductivity meter. The conductivity meter displays both electrical conductivity (EC) and total dissolution solids (TDS) results. This meter possesses a temperature sensor and conductivity probe. The probe is labeled with a cell constant. Before every measurement, the probe tip was rinsed with distilled water and the sample, and after immersing the conductivity probe into the sample for a measurement, the sample was stirred with a glass bar to achieve an ideal condition for an accurate answer.

2.13. Chemical Oxygen Demand (COD) Analysis

This analysis was carried out using Lovibond water testing RD 125 and Lovibond water testing Photometer-System MD 200. The RD 125 is the reactor used to digest the vial after mixing each with 2 ml of the samples and one with distilled water used as a blank for 120 minutes at a temperature of 150 °C or less.

2.14. Adsorbent Recycling and Regeneration

Recycling is the process of processing materials that would have otherwise been thrown away as trash into new products, which minimizes production costs as well. This phenomenon in the adsorption process is termed desorption. Desorption is simply using an eluent to create sorption equilibrium or destabilize the bond between the pollutant (bulk phase) and the adsorbing surface. Different desorption methods, including chemical regeneration, thermal regeneration, thermochemical regeneration, steam regeneration, bio-regeneration, vacuum regeneration, electrochemical regeneration, pressure swing regeneration, ozone regeneration, microwave regeneration, oxidative regeneration, and ultrasound regeneration, have been used in the regeneration or recycling of adsorbents. In this research, a chemical regeneration method was employed, and the eluents used were acid and base.

2.15. Batch Desorption

The exhausted adsorbent was mixed with the eluent and stirred at a specific temperature for 30 minutes per cycle until equilibrium was reached. It was then filtered into filtrate and residue adsorbent at the end of each cycle. The filtrate was for dye analysis using a UV spectrophotometer for desorption efficacy, while the residue sorbent was washed with water to remove the eluting agent, which was then oven dried and kept for reuse in a fresh process. The amount (quantity) in mg/g and efficacy in % of desorbed adsorbate (pollutant) were calculated using equations (30) and (31), respectively.

$$\text{Amount /quantity desorbed (mg/g)} = A_{des} = \frac{C_s * V}{M} \tag{30}$$

$$\text{Efficiency of desorbed (\%)} = \%_{des} = \frac{A_{des}}{C_{ad}} X\ 100 \tag{31}$$

Where, C_s is concentration of adsorbate desorbed in mg/g, C_{ad} is concentration of adsorbate adsorbed in mg/g, M is weight of exhausted adsorbent in gram and V is volume of the eluent in liter.

3. RESULTS AND DISCUSSION

3.1. Characterization Results

3.1.1. FTIR analysis

Figure 3a, b, and c presents the FTIR spectra of raw Umuahia clay (RUC), acid modified (H_2SO_4) Umuahia clay (AUC) and CR adsorbed on AUC. From spectra of Figure 3a, higher no of peaks was observed than in Figure 3b which may be as a result of acid modification that removes impurities contained in the raw clay material and the peaks of Figure 3b composed of various functional groups which are responsible for binding of CR dye e.g. Amide, alkane, alcohol, alkyne halide. Figure 3c also showed spectra of higher peaks than Figure 3b as well which indicate the possible involvement of some functional groups on the surface of the AUC in the adsorption process.

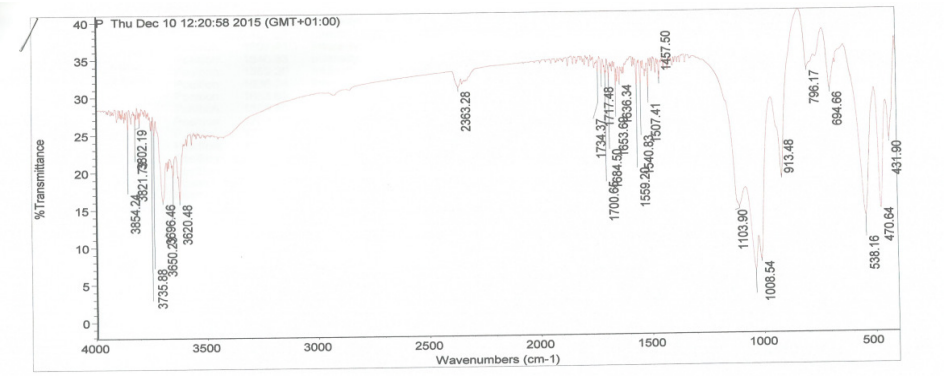

Figure 3a: FTIR of raw Umuahia clay

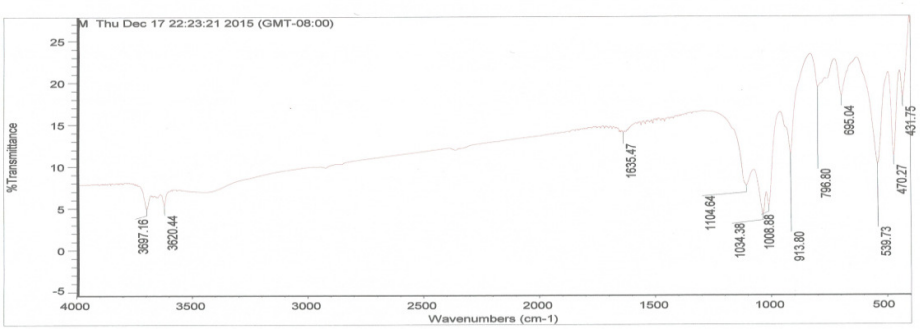

Figure 3b: FTIR of activated Umuahia clay

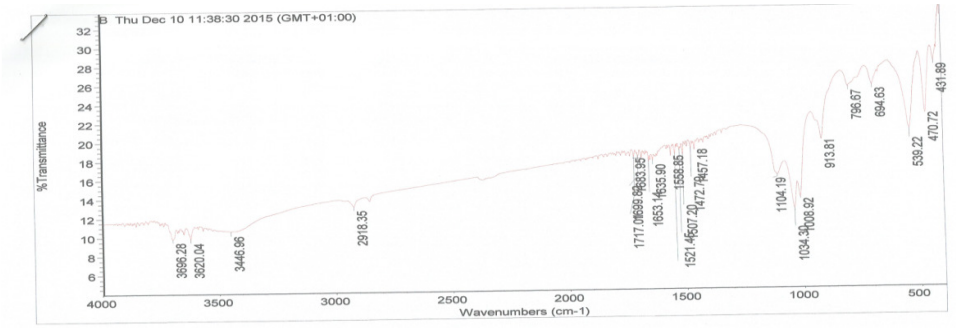

Figure 3c: FTIR of after CR adsorption

3.1.2. SEM micrographs

Figure 4a, b, and c present the scanning electron micrograph (SEM) of Umuahia clay samples at raw state, activated state and after CR adsorption on AUC state. Figure 4b clearly displayed considerable number of heterogeneous layer of pores and internal surface of the clay material than Figure 4a, this observed development is as a result of modification which exposed the internal surface of the clay sample. Figure 4c showed a smoother surface which signified adsorption been taken place. The observed smooth surface is dye particles that cover most porous surfaces of Figure 4b.

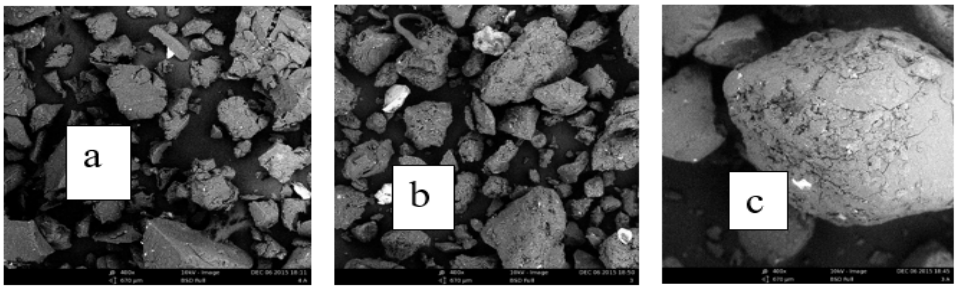

Figure 4: SEM Micrograph of: (a) raw clay, (b) activated clay, (c) after adsorbed clay

3.2. Batch Adsorption Studies

3.2.1. Effect of particle size

The effect of particle size was studied with particle sizes range of 50, 75, 150, 300 and 600 µm at a constant temperature of 333 k, an adsorbent dosage of 0.5 g, initial dye concentration of 100 mg/l, a time of 60 min, and a pH of 2. The result of the study as reported in the histogram of Figure 5a, shows that the percentage dye adsorption increases with sorbent decreased in particle size, from 65.9% at 600 µm to 98.2% at 50 µm,

this is because smaller particles possess a larger surface area and pores than bigger particle size. Additionally, the breaking of larger particles opens tiny cracks and channels on the particle surface of the material, resulting in more accessibility and easy diffusion due to the smaller particle size. The outcome of this study concurs with the previous report by Oguanobi et al., (2019) who confirmed that an increase in adsorbent particle size distinctly decreased the percentage of dye removed. El-Halwany, (2010), and Wu et al., (2012) also reported that dye removal increased with the decrease in particle size.

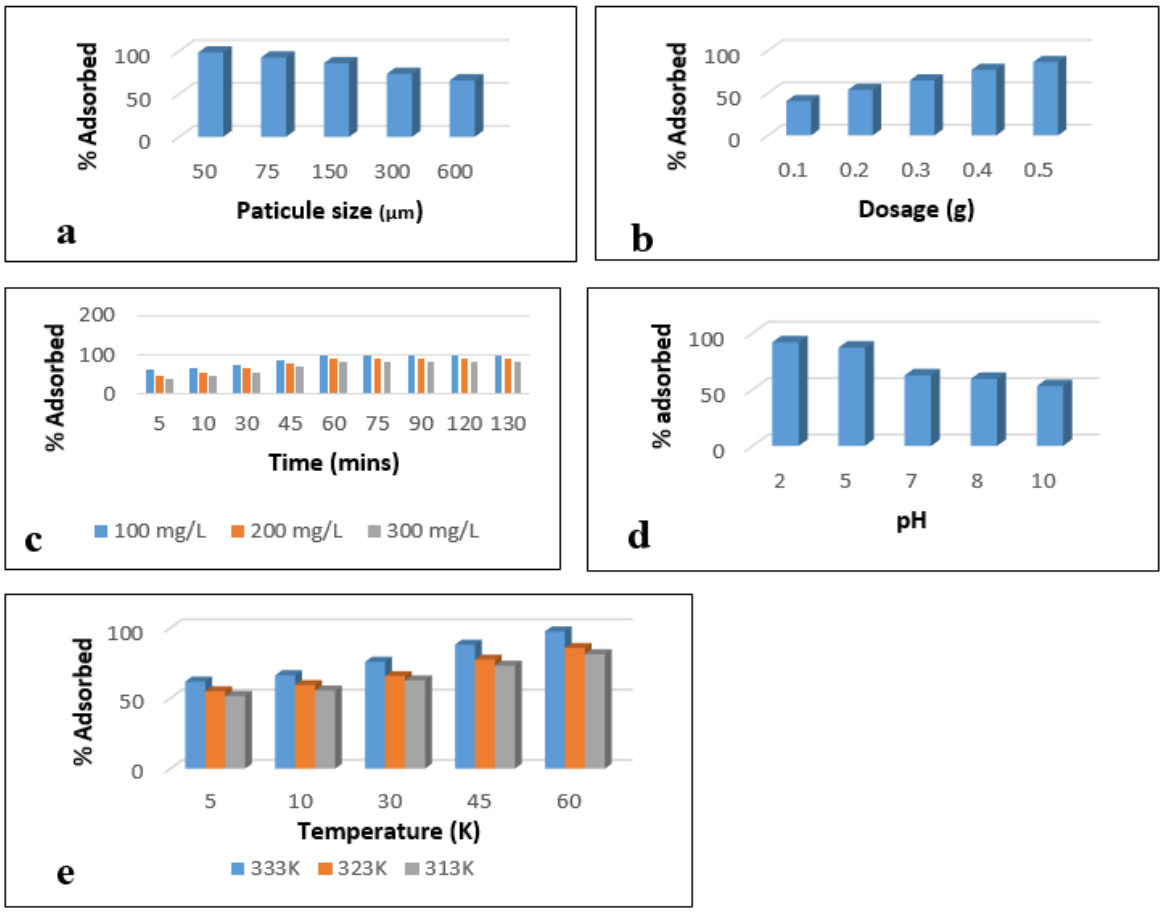

Figure 5: Effects of process parameters displaying impact of (a) particle size, (b) dosage, (c) time and concentration, (d) pH, and (e) temperature and time on the percentage of CR adsorbed

3.2.2. Effect of adsorbent dosage

The adsorbent dosage effect was investigated for the dosage range of 0.1, 0.2, 0.3, 0.4, and 0.5 g/100 ml of CR at a constant temperature of 313 k, an adsorbent particle size of 50 µm, a pH of 2, an initial dye concentration of 100 mg/l, and a time of 60 min. The result of the study, as reported in the histogram in Figure 5b, shows that the percentage of adsorption increases with an increase in adsorbent dosage, from 40.6% at 0.1 g to 86.7 at 0.5 g. The observed increase in percentage adsorption of dyes per increase in adsorbent dosage is a result of the increased surface area of active functional groups, which also gives rise to a greater availability of adsorption sites (Ladhe et al., 2011, Oguanobi et al., 2019). Moreover, as the adsorbent dosage increased, a significant decrease in the amount adsorbed per unit mass of the adsorbent was observed. This decrease in unit adsorption as adsorbent dosage increases is a result of adsorption sites remaining unsaturated during the adsorption process. The result of this research concurs with the previous

reports by Oguanobi et al., (2019) and Ismat et al., (2023) and, who reported that an increase in HAC dosage drastically decreased the amount of crystal violet dye in the aqueous solution.

3.2.3. Effect of concentration and contact time

The effect of initial dye concentration was studied at concentration ranges of 100, 200, and 300 mg L^{-1} per 0.5 g adsorbent dosage at a contact time range of 5–130 minutes at a constant temperature of 333 k, an adsorbent particle size of 50 µm, and pH 2. The result, as reported in Figure 5c, shows that the amount of CR adsorbed per unit mass increased with an increase in initial ion concentration, whereas the adsorption percentage decreased. This outcome is due to the proportion of the initial number of dye molecules to the available surface area at low concentration. Moreover, an increase in the amount or percentage of adsorption as contact time increases at all initial concentrations until equilibrium was observed. This accounts for the driving force provided by the initial dye concentration to overcome the resistance to the mass transfer of dye between the adsorbate and the adsorbent. Finally, a three-step stage was observed during the adsorption reaction: the bulk diffusion stage (a rapid initial adsorption), the pore diffusion and intra-particle diffusion stage (a period of slower uptake), and the equilibrium stage (a period of no significant uptake). The findings of this study are consistent with those of Barakan et al., (2019) and Oguanobi et al., (2019), who found that at higher ion concentrations of As (V) and CV^{+}, adsorption efficiency decreased due to a decrease in available active sites. Mahmoud et al., (2019) also reported that the equilibrium of the PNP adsorption on the montmorillonite clay was reached after 120 min.

3.2.4. Effect of pH

The effect of pH is paramount when the adsorbing molecules are capable of ionizing in response to pH. CR is a diazo/anionic dye and maintains its red color at pH 5, while below pH 2, the solution changes from red to dark blue; at pH 3, it changes to blue-violet; and the original red color is different above pH 10. The pH effect is studied between the pH ranges of 2 and 10, at a constant temperature of 313 k, an adsorbent particle size of 50 µm, an initial dye concentration of 100 mg/l, a time of 60 min, and an adsorbent dosage of 0.5 g. The result of the study, as reported in the histogram of Figure 5d, shows that the highest removal efficiency of 91.9% was achieved at pH 2, which is due to the very low solubility of CR at pH < 2. Low pH leads to an increase in H^{+} ion concentration in the system, and the surface of the clay acquires a positive charge by adsorbing H^{+} ions. As the clay surface is positively charged at a low pH, a significantly strong electrostatic attraction appears between the positively charged sites and the anionic dye molecules. A negatively charged surface site on the clay does not favor the adsorption of anionic CR molecules due to electrostatic repulsion. The findings of this study concur with previous reports by Reddy et al., (2011), Adebayo et al., (2022), and Imessaoudene et al., (2023), who found that pH 2 was optimal for removing Congo red Indian Jujube Seeds (IJS) (Zizyphus maruritiana) and using CHCFe. Lafi et al., (2019) and Popoola et al., (2021) also reported optimum pH 3 for the removal of Congo red using activated coffee waste and synthesized coal graphene. Moreover, Mahmoud et al., (2019) reported that the PNP adsorption on montmorillonite is pH-dependent.

3.2 5. Effect of temperature

Temperature as a process variable studies the adsorption thermodynamics and nature, i.e., whether a system is an exothermic or endothermic process. The impact of temperature on CR uptake was examined using a temperature range of 313K, 323K, and 333K at a constant adsorbent dosage of 0.5g, an adsorbent particle size of 50 µm, an initial dye concentration of 100 mg/l, a pH of 2, and a time period of 60 minutes. The result, as reported in the histogram of Figure 5e, shows an increase in the amount of CR uptake from 81.4% to 97.5% as the temperature of the solution increases. This outcome confirms the adsorption process of CR on AUC as an endothermic system. The observed increase in CR uptake is a result of an increase in the mobility of dye molecules, which may also cause enlargement and disintegration of the internal structure of the adsorbent, thereby enabling large dye molecules to penetrate further. The obtained result is in harmony with the previous report by Oguanobi et al., (2019), who reported that CV^{+} adsorption on HAC is more energetically favorable to occur at higher temperatures. Mahmoodi et al., (2011), Salleh et al., (2011) and Mahmoud et al., (2019), also reported similar results of the same trend.

3.3. Equilibrium Modeling

The equilibrium adsorption represents the relationship between the mass of adsorbate adsorbed per unit weight of adsorbent and the liquid-phase equilibrium concentration of the adsorbate (Lata et al., 2007). The non-linear expression of Langmuir, Freundlich, Vieth-Sladek, Dubinin-Radushkevich, Redlich-Peterson, and Jovanovic isotherms was used to analyze equilibrium results. The result in graphical form is reported in Figure 6. The respective constants of each model were evaluated using software and tabulated in Table 3.

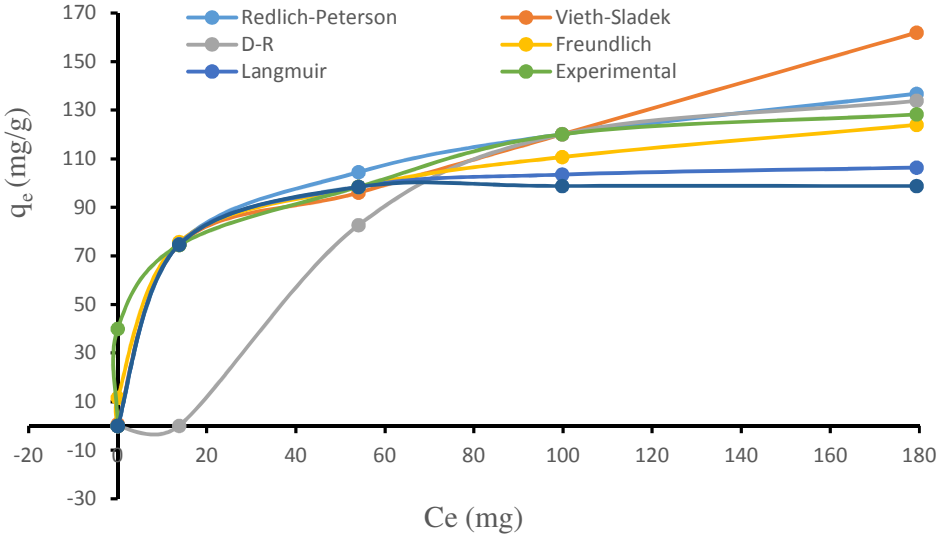

Figure 6: Non-linear isotherm plot for adsorption CR on AUC

From Table 3, it's seen that Langmuir maximum adsorption capacity (Q_m) value is 98.7447. The K_L Value of 5.0422 indicates that the adsorbate molecules have a high affinity for the adsorbent surface (strong adsorption) and the R_L value of 0.000396 as seen in Table 3, certifies favorable uptake of CR dye. The Freundlich equation is an empirical relationship between the amounts of adsorbate molecules adsorbed onto heterogeneous surfaces. From Table 3, the n_f value of 5.195 indicates that the adsorption sites have non-uniform energies and thereby classify the surface as more heterogeneous. The obtained n_f value also confirms the uptake of CR dye as a favorable physical process. The high n_f value of 5.195 confirm good affinity of the adsorbate for the adsorbent. The Vieth-Sladek isotherm is used for estimating diffusion rates in solid materials from transient adsorption. From Table 3, a significant k_{vs} value of 0.5255 certifies that the adsorbent has a strong affinity for the gas molecule, whereas a significant B_{vs} value of 14.9975 suggests good interaction between adsorbed molecules. The Dubinin-Radushkevich (D-R) isotherm is a temperature-dependent model that forecasts the adsorption mechanism. An adsorption process is physical when the "E" value is below 8 kJ mol^{-1} and chemical, when the "E" value is within the range of 8–16 kJ/mol (Kausar et al., 2013, Singha and Das, 2013). From Table 3, "E" values as seen lie within the range 0-8 KJ mol^{-1} thereby confirming the uptake process of CR dye physical adsorption. The b_{DR} value as seen in Table 3 is very small, thereby suggesting a narrow energy distribution and probably a possible homogeneous system. The Redlich-Peterson model embodied both the Freundlich and Langmuir isotherm features. From Table 3, the g value of 0.7868 suggests monolayer adsorption on a homogeneous adsorbent surface. The g value also suggests that the gas deviates more from ideal gas behavior to a real gas due to stronger intermolecular forces. This is because the deviation from ideal behavior is more pronounced. The a_R value of 1.8658 indicates that the adsorbent has a good ability to adsorb and retain more adsorbate molecules at a given temperature. The K_R value of 85.1934, indicates that the adsorbent has a great adsorption capacity and affinity for the adsorbate. The Jovanovic model presumes superficial adsorption and mechanical interaction between the adsorbate and the adsorbent surface. The K_J value of 0.1019 indicates good adsorption affinity of the adsorbate for the

adsorbent. The high Q_m values of Langmiur, D-R, Vieth-Sladek, and Jovanovic, validate the outcome of other parameters likeK_L, $K_{R,}$, n_f, and K_J which confirm the good affinity of the adsorbent for the adsorbate.

Table 3: Calculated isotherm and kinetic Parameters for the Adsorption of CR on AUC

Isotherm		Kinetic	
$q_{e(exp)}$ = 39.9997			
Langmuir		Pseudo-First order	
Q_m	98.7447	q_{ecal}	39.93
K_L	5.0422	K_1	0.0477
R_L	0.000396	Ho	1.9056
NSD	3.6799	NSD	1.2279
ARE	2.9439	X^2	0.0091
Freundlich		Pseudo-Second order	
K_F	45.6451	q_{ecal}	39.7969
n_F	5.195	K_2	0.0027
NSD	2.2195	Ho	4.2870
ARE	01.7756	NSD	4.1188
		X^2	0.4246
Vieth-sladek			
Kvs	0.5255	Pseudo-nth order	
Q_m	67.6958	q_{ecal}	39.9544
Bvs	14.9975	Kn	0.0599
NSD	0.4191	N	0.9136
ARE	0.3353	NSD	1.0185
		X^2	0.0034
D-R			
Q_m	140.5261	Avrami	
b_{DR}	0.000206	q_{ecal}	39.7962
E	49.2419	Kav	0.0476
NSD	6.7552	Nav	1.0175
ARE	5.4042	NSD	1.2658
		X^2	0.0127
R-P			
K_R	85.1934	Elovch	
a_R	1.8658	β	0.2560
G	0.7868	α	311.47
NSD	1.3541	NSD	3.5441
ARE	1.0833	X^2	0.8236
Jovanovic		Fractional Power	
Q_m	98.7846	K	15.0837
K_J	0.1019	V	0.2060
NSD	4.9150	NSD	2.4044
ARE	3.9320	X^2	0.1778

3.4. Kinetic Modeling

Adsorption kinetics refers to the study of the rate (how fast or slow) at which an adsorbate (a gas molecule) is adsorbed onto an adsorbent (a solid surface) under specific conditions. For evaluating the adsorption kinetics of CR onto AUC, pseudo-first-order, pseudo-second-order, Elovich, fractional power, Avrami, and pseudo-nth-order kinetic models were used to fit the experimental data. The pseudo-kinetic models assume that adsorption is a pseudo-chemical reaction. When the adsorption processes occur through chemisorption, the Elovich model is most commonly used (Dotto and Pinto, 2011). The curve fittings of the models are presented in Figure 7. The values of the respective constants of the non-linear model were evaluated using Excel software and tabulated in Table 3.

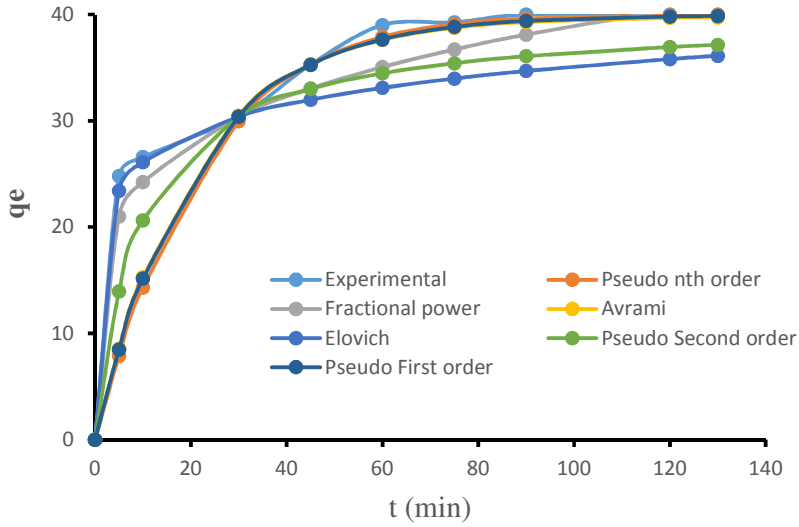

Figure 7: Non-linear kinetic plot for adsorption of CR on AUC. (A plot of q_t against t)

From Table 3, the smaller K_1 value of 0.0477 for pseudo-first order suggests a slow adsorption process, while the smaller K_2 value of 0.0027 for pseudo-second order confirms zero correlation with the dye initial concentration, indicating that more than one adsorption mechanism controls the uptake of CR. The pseudo-nth- order constant "n," which provides information on the reaction order, and a smaller n value of 0.9136 suggest a negative order, thereby indicating that the reaction rate is less susceptible to changes in the reactant concentration. The smaller K_n value of 0.0599 indicates a slower reaction rate. This outcome is in agreement with the prediction of K_1 parameter of pseudo-first order, which also confirms the slow adsorption process. The H_o constant of pseudo-first and second order calculates the initial adsorption rate, and the values obtained theoretically are quite in agreement with the experimental date. The calculated qe values obtained from pseudo-first order, pseudo-second order, pseudo-nth order, and Avrami kinetic models are in close agreement with the experimental qe value. The Elovich model constant β is the desorption constant. The β values of 0.2560 indicate that the adsorption of CR onto AUC is reversible. The α value of 311.47 suggests a faster initial adsorption rate, meaning that AHC has a high affinity for CR dye. This outcome concurs with the initial stage of the adsorption process, "a rapid initial adsorption," as classified by Weber-Morris, (1963).

3.5. Error Function Statistical Analysis

The best fit of the studied model for the uptake of CR dye on AUC was evaluated using the error parameter of the non-linear regression expression of equations 24 and 28 for equilibrium model assessment, while equations 28 and 29 are used for kinetic model assessment. In non-linear regression, the rule for goodness of fit assessment is that the smaller the obtained value of the error function, the better the curve fits. The obtained results of the isotherm models as tabulated in Table 3 show that all the theoretical equilibrium

models, with the exception of the D-R model, follow the adsorption of CR dye based on the non-linear regression rule, but the Vieth-Sladek model gives the best fit to the experimental values for the uptake of CR dye on AUC after fulfilling the rule for goodness of fit assessment of non-linear regression by giving the smallest values of 0.4191 and 0.3353 for the error functions NSD and APE. The obtained results of the kinetic models, as shown in Figure 7 and tabulated in Table 3, show that all the theoretical kinetic models follow the adsorption of CR dye, but the pseudo-nth-order model gives the best fit to the experimental values for the uptake of CR dye on AUC after fulfilling the rule for goodness of fit assessment of non-linear regression by giving the smallest values of 1.0185 and 0.0035 for the error functions NSD and used for statistical analysis. The good fit of pseudo-nth order was confirmed by the calculated qe value, which is in close agreement with that of experimental data.

3.6. Adsorption Mechanism

3.6.1. Intra-particle diffusion model

The intra-particle diffusion model was proposed by Weber-Morris to identify the adsorption mechanism and predict the rate-controlling step. This model usually includes three steps. The first step is external surface adsorption or boundary layer diffusion. The second step is the gradual stage of adsorption, which is intra-particle diffusion. The third step is the final equilibrium stage, in which the intra-particle diffusion starts to slow down due to the extremely low dye concentration left in the solution. However, if the data exhibit multi-linear plots, then two or more steps influence the sorption process. The intercept of the linear plot of qt versus $t^{1/2}$ in (mg g-1) signals an idea about the thickness of the boundary layer, and the larger the value of the intercept, the greater the boundary layer effect (Srivastava et al. 2006). If the plot is linear and passes through the origin, then intra-particle diffusion is the rate-controlling step. The intra-particle diffusion model can be expressed as follows:

$$q_t = K_{id}\sqrt{t} \tag{32}$$

Where q_t (mg/g) is the amount of adsorbate adsorbed at time t, and k_{id} ($mgg^{-1}min^{1/2}$) is the intraparticle constant obtained from the slope of q_t versus $t^{1/2}$.

Figure 8a shows that the linear plot did not pass through the origin, which indicated that the intra-particle diffusion was not the only rate-controlling step and that the boundary layer diffusion controlled the adsorption to some degree (Cheung et al., 2007). This deviation may be due to the difference in mass transfer rate in the initial and final stages of adsorption (Hameed and Hakimi, 2008). Furthermore, the data, as seen in Figure 8a, exhibit multi-linear plots, which indicates that two or more steps influence the sorption process. Comparing the k_{id} values for the macropore and micropore diffusion stages for CR uptake shows that the rate-limiting step is the micropore diffusion stage because the micropore diffusion constant $k_{id}2$ value of 0.2786 is lower than the macropore diffusion constant $k_{id}1$ value of 2.2137. This outcome confirmed the rate of micropore diffusion in the slower step and the rate-determining step. Moreover, the higher value of $k_{id}1$ also indicates that the uptake of CR onto the AUC was largely controlled by the intraparticle diffusion model. The boundary layer effect, i.e., the intercept of the micropore diffusion stages from Figure 8a, is 36.96, which further shows a greater effect than the macropore stage with an intercept of 19.5. The non-zero intercept of the plot at both the micropore diffusion and macropore diffusion stages is a clear indication that although intra-particle diffusion is slow, it is not the slowest of the rate processes that determines the overall order, thus it cannot be stated that the intra-particle diffusion process is the rate-limiting step occurring during the sorption of CR onto AUC.

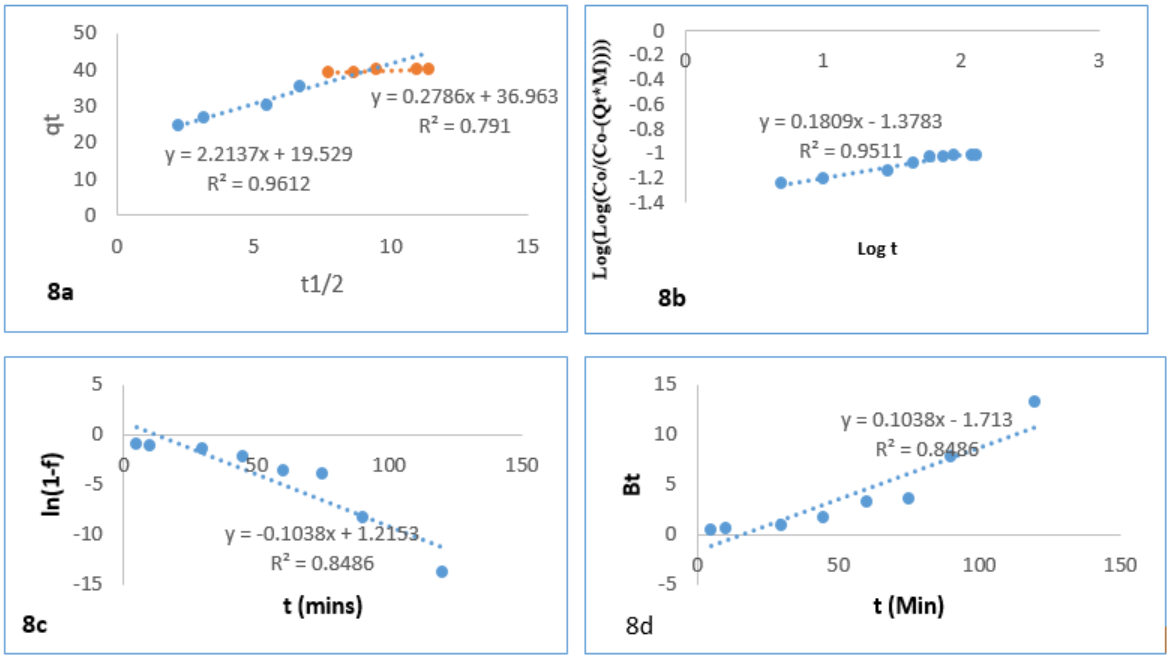

Figure 8: Adsorption mechanism plot of different model (a) Intra-particle diffusion plot, (b) Bangham model plot, (c) Liquid film model plot, and (d) Boyd diffusion model plot

3.6.2. Bangham pore diffusion model

The Bangham pore diffusion model is an empirical model that investigates adsorbate pore diffusion activities, and it does so by calculating whether pore diffusion controls or dominates the adsorption process. The Bangham model can be expressed as follows:

$$Log\ Log\left(\frac{C_i}{C_i - q_t M}\right) = Log\left(\frac{K_J M}{2.303V}\right) + \alpha Log t \tag{33}$$

Where C_i, is the initial concentration (mg/L), V (mL) is the volume of the solution, M is the mass of the adsorbent (g), q_t is the amount of adsorbate adsorbed at time t. K_J and α are Bangham pore constants which can be obtained from intercept and slope of the plot of Log(Log(Co/(Co-(Qt*M)))) versus Log t (double logarithm plot).

In Figure 8b, the Bangham plot gives a nonlinear curve for the dye removal, indicating that the diffusion of adsorbate into the pores of the adsorbent is not the only rate-controlling step. Additionally, the nonlinear curve indicates multiple adsorption stages, which validates the intra-particle diffusion model that has previously indicated that two or more steps influence the sorption process. The correlation coefficient value of 0.9511 obtained from the Bangham model suggests that pore diffusion was involved in CR uptake onto AUC, but not the sole rate-controlling step.

3.6.3. Liquid film diffusion model

The liquid film diffusion model was also used in this study to investigate if transport of dye from the liquid phase up to the solid phase boundary also plays a role in the adsorption process. The liquid film diffusion model can be expressed as follows:

$$-\ln(1 - F) = -K_{fd} t \tag{34}$$

Where F is the fraction of solute adsorbed at equilibrium, K_{fd} is the liquid film diffusion constant, and F value can be evaluated using

$$F = \frac{q_t}{q_e} \tag{35}$$

Where q_t and q_e are the amount dye adsorbed on the adsorbent at any time *t* and at equilibrium respectively.

A linear plot of ─ ln (1─F) versus t with zero intercept would suggest that the kinetics of the sorption process was controlled by intra-particle diffusion through the liquid surrounding the solid sorbent. Figure 8c shows that the intercept of the liquid film plot is above zero (origin) but close to the origin (zero), which indicates the significance of liquid film diffusion in the rate determination of the adsorption process (Srivastava et al. 2006), and the kinetics are likely to be diffusion-limited. However, the regression coefficient (R^2) value of 0.8486 is quite lower than 0.9612 for intra-particle diffusion; this indication shows film diffusion was involved in the adsorption process but not as a rate-determining factor. Moreover, the liquid film diffusion rate constant (K_{fd}) value of -0.1038 is insignificant as compared with the intra-particle rate constant (kid), which is an indication that the liquid film diffusion process was not the rate-limiting step occurring during the sorption of CR on the AUC.

3.6.4. Boyd pore model

The Boyd model is an empirical equation that also gives insight into the mechanism of adsorption. This model is applied to determine the rate-controlling step (the slow step involved) for the adsorption process. The Boyd model can be expressed as follows:

$$F = 1 - \left(\frac{6}{\pi^2}\right) exp^{(-Bt)} \tag{36}$$

$$Bt = -0.4977 - \ln(1 - F) \tag{37}$$

Where *Bt* is the function of *F* and *F* is the fraction of solute adsorbed at different times, *t*. The *Bt* values at different contact times, *t*, can be evaluated using equation 37 in the case of $F > 0.85$. The *F* value can be calculated using equation 26.

$$F = \frac{q_t}{q_e} \tag{35}$$

Where q_t and q_e are the amount dye adsorbed on the adsorbent at any time *t* and at equilibrium respectively.

Cáceres-Jensen et al., (2013) proposed that if the plot of *Bt* versus *t* is a straight line and passes through the origin, it is the pore diffusion that controls the rate of mass transfer (or particle diffusion mechanism). In contrast, if the plot is nonlinear or linear but does not pass through the origin, film diffusion or external mass transport will be the major dominating factor (Cáceres-Jensen et al., 2013). Figure 8d shows that the Boyd plot is linear but did not pass through the origin, which demonstrated that intra-particle diffusion was not the solely controllable process and that diffusion-chemisorption might be more rational to explain the adsorption of CR dye ions on AUC.

3.7. Thermodynamic Study

The variation of dye removal efficiency with respect to temperature shall be explained by the thermodynamic parameters, such as ΔG^o, ΔH^o and ΔS^o (Hu et al., 2010), which are evaluated from Equation. (15–18). The plot of In K_C versus T^{-1} of the CR adsorption process is carried out as indicated in Figure 9a, in which the slope and intercept obtained by a curve-fitting program are used to calculate the ΔH and ΔS.

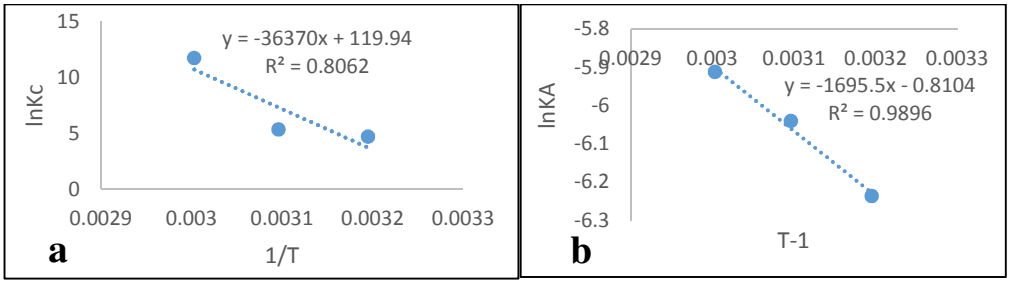

Figure 9a and b, Plot of lnKc and lnK_A against T^{-1} for the removal of CR by clay adsorbent

The slope of the plots is equal to $-\Delta H^o/R$, and its intercept is equal to $\Delta S^o/R$. The calculated parameters of ΔG, ΔH and ΔS are shown in Table 4.

Table 4: Thermodynamics parameters for the adsorption of CR on AUC

Temp (K)	InK_c	ΔG (KJ/MOL)	ΔS (J/MOL)	ΔH (KJ/MOL)	E_a (KJ/MOL)
313	4.696	-12.2203	997.1812	302.38	14.0964
323	5.3606	-14.3955			
333	11.7361	-32.4921			

The negative values of ΔG indicate that adsorption is spontaneous, the positive value of ΔH indicates that the adsorption process is endothermic, and the positive value of ΔS suggests increased randomness at the solid or solution interface during the adsorption of CR on AUC and corresponds to an increase in the degree of freedom of the adsorbed species (Dalia et al., 2011). Thus, adsorption is favored on CR. Reddy et al., (2011) reported a similar phenomenon in the removal of Congo red from an aqueous medium using jujuba seed.

3.7.1. Activation energy

The magnitude of the activation energy yields information on whether the adsorption is mainly physical or chemical. The physisorption process normally had an activation energy of 5–40 KJ/mol, while chemisorption had a higher activation energy (40–800 KJ/mol) (Wu, 2007). In order to evaluate the activation energy of adsorption, the Arrhenius equation was applied using the relationship of Equation. 19. Figure 9b shows the plot of the activation energy of CR on the AUC adsorbent, and Table 4 presents the calculated Ea values for the adsorption. It is clearly observed from Table 4 that the Ea value for CR adsorption on AUC is positive and below 40 KJ mol^{-1}, thus indicating that adsorption of CR using AUC is feasible and a physisorption process. This phenomenon concurs with the Freundlich constant "n_f" result, which referred to the process as physical. A similar phenomenon was reported on the adsorption of basic dye using acid-treated kenal fiber char (Dalia et al., 2011).

3.8. Optimization using Response Surface Methodology

3.8.1. ANOVA analysis for CR removal

A design expert was used to analyze the result, and the summary of the P-value and the model summary statistics are presented in Table 5.

Table 5: Statistical summary of the models investigated

Source	Df	Standard deviation	R-squared	Adjusted R^2	Predicted R^2	PRESS
Linear	4	2.93	0.7040	0.6566	0.5493	324.67
2FI	6	2.27	0.8614	0.7884	0.6606	244.50
Quadratic	4	0.6166	0.9921	0.9847	0.9567	31.16
Cubic	8	0.2879	0.9992	0.9967	0.8957	75.12

The quadratic model for optimum point prediction of the process was suggested from the CCD module with high R-squared, adjusted R^2 and predicted R^2 values of 0.9921, 0.9847 and 0.9567, respectively. Table 6 presents the analysis of variance (ANOVA) and it confirmed the adequacy of the quadratic model.

Table 6: ANOVA and model coefficients for CR adsorption

Source	Sum of squares	df	Mean squares	F-value	p-value Prob>F
Model	714.71	14	51.05	134.27	< 0.0001
A-Temperature	7.42	1	7.42	19.51	0.0005
B-Concentration	20.92	1	20.92	55.03	< 0.0001
C-Ph	171.77	1	171.77	451.78	< 0.0001
D-Dosage	307.03	1	307.3	807.54	< 0.0001
AB	0.0046	1	0.0046	0.0120	0.9143
AC	0.2426	1	0.2426	0.6380	0.4369
AD	2.58	1	2.58	6.80	0.0198
BC	0.1008	1	0.1008	0.2651	0.6141
BD	3.18	1	3.18	8.36	0.0112
CD	107.28	1	107.28	282.16	< 0.0001
A^2	0.9104	1	0.9104	2.39	0.1426
B^2	0.3200	1	0.3200	0.8417	0.3734
C^2	17.20	1	17.20	45.25	< 0.0001
D^2	51.55	1	51.55	135.59	< 0.0001
Residual	5.70	15	0.3802		
Lack of fit	5.65	10	0.5655	28.25	< 0.0002
Pure error	0.0485	5	0.0097		
Cor total	720.4	29			

Significant terms of the model are checked from F-values and P-values. The higher the F-value, the smaller the P-value, and the more significant the corresponding coefficient. The higher model F-value of 134.27 implies that the model is significant, and P-values whose coefficients are less than 0.05 are significant terms; therefore, A, B, C, D, AD, BD, CD, C2, and D^2 are significant terms. A similar phenomenon was reported by Amini et al., (2008). The empirical correlation between the variables (response and independent) in the coded form on the basis of the experiment results was reported as follows:

$$Y_{AUC}\,(\%) = +98.77 + 0.6069A - 1.02B - 2.93C + 3.92D - 0.4019AD + 0.4456BD + 2.59CD - 1.36C^2 - 2.35D^2 \quad (36)$$

The good fit of the model equation was validated using R^2 (coefficient of regression). The high coefficient of regression value of 0.9992 implies that 99.92% of the variability in the response can be explained by the model.

3.8.2. RSM Graphical Plots

This plot shows the relationship between the actual and predicted values of the response. As seen in Figure 10, all the data points were closely assembled to the straight line of a coefficient of regression of 0.9992, which implies a good correlation between the actual and predicted values of the response. The high coefficient of regression value certifies that the prediction of the quadratic model is correct in describing the removal of dye from an aqueous solution. A similar phenomenon was reported by Iheanacho et al., (2019) and Onu and Nwabanne, (2014).

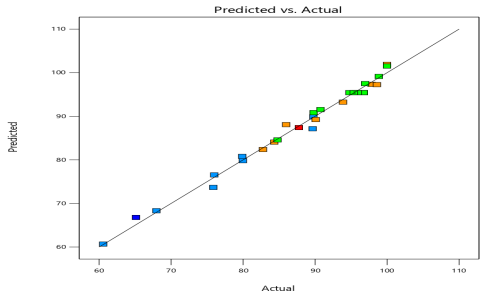

Figure 10 Plot of the experimental and predicted response

The 3D surface plots represent the effect of two process variables on the adsorption of CR. Figure11a-c, reveals the relationship between every two independent process variables. The spherical nature of the contour in the graphs shows that there was a mutual significance between every two variables.

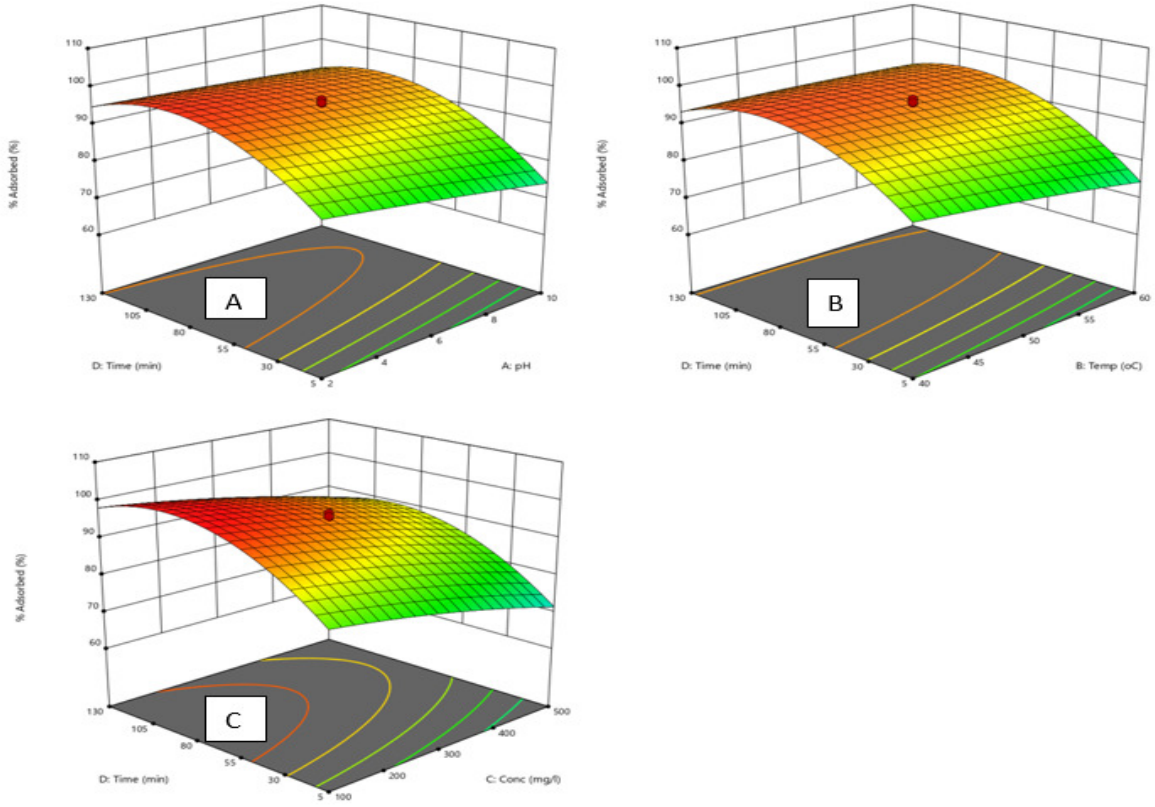

Figure 11. 3D surface plot for CR adsorption on the adsorbent showing combined effects of (A) Time and pH, (B) Time and Temperature, and (C) Time and concentration

3.9. ANN Modeling and Prediction

The artificial neural network for the adsorption of CR was modeled using the neural toolbox of MATLAB software. The best ANN with input, hidden, and output nodes of 4, 9, and 1, respectively, was used to model the optimum percentage removal of CR in the adsorption process. The input nodes represent the independent variables, while the output nodes represent the response. The hidden layers show the nonlinear

transformations in the input space. The optimal number of neurons in the hidden layer was determined by varying the number of neurons in the hidden layer and comparing the mean square error obtained. Therefore, the ANN topology architecture of 4-9-1, corresponding to the four input variables (temperature, concentration, pH, and adsorbent dosage), nine neurons in the hidden layer, and one output variable (percentage adsorbed), was used in the ANN modeling. Levenberg-Marquardt (LM) back propagation was the algorithm utilized in the ANN modeling. The properties of ANN modeling are algorithm, error function, input layer neuron, hidden layer neuron, output layer neuron, training, hidden layer, and data division. The validation of the neural network process at the 6th epoch iteration was achieved using the ANN validation performance plot in Figure 12, and the lowest mean square error of 3.09×10^{-3} was observed.

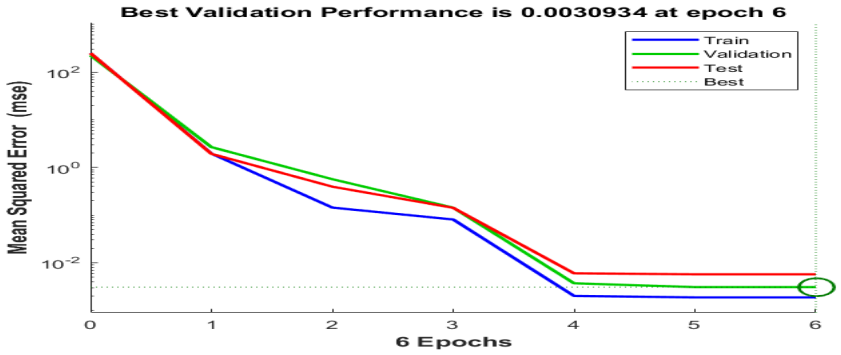

Figure 12: ANN validation performance plot

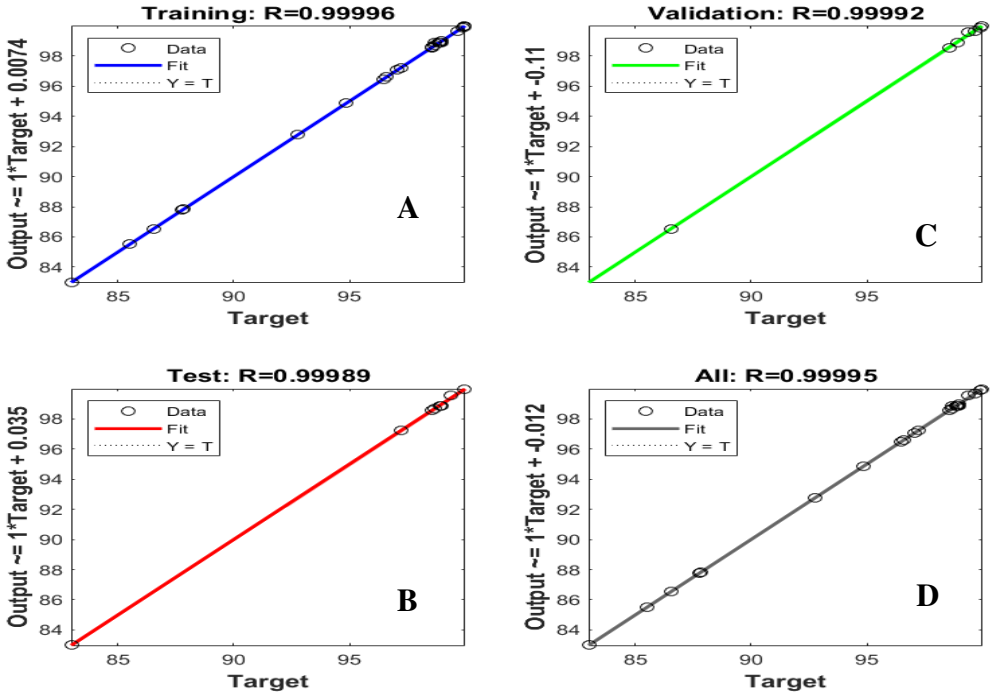

Figure 13: ANN regression plots for (A) training, (B) test, (C) validation and (D) overall **process**

The experimental data were divided into training, testing, and validation so that the number of parameters in the model would not exceed the size of the training dataset. Scatter diagrams that compared experimental data (target) with the computed neural data for training, testing, validation, and overall data are shown in Figure 13. The regression values of 0.99996, 0.99889, 0.99992, and 0.99995 were obtained for the training, testing, validation, and all (overall) data, respectively. These high coefficients of regression explain the nature of the neural fittings. Moreover, the outputs were very close to the targets, as most of the data points were assembled along the straight line of the coefficient of regression. The percentage predicted CR removal of the ANN model is presented in Table 7.

3.10. ANFIS Modeling and Prediction

Four input parameters (temperature, concentration, pH, and adsorbent dosage) were utilized to predict the percentage of CR dye removal using the ANFIS model. Figure 14 shows the ANFIS Sugeno diagram.

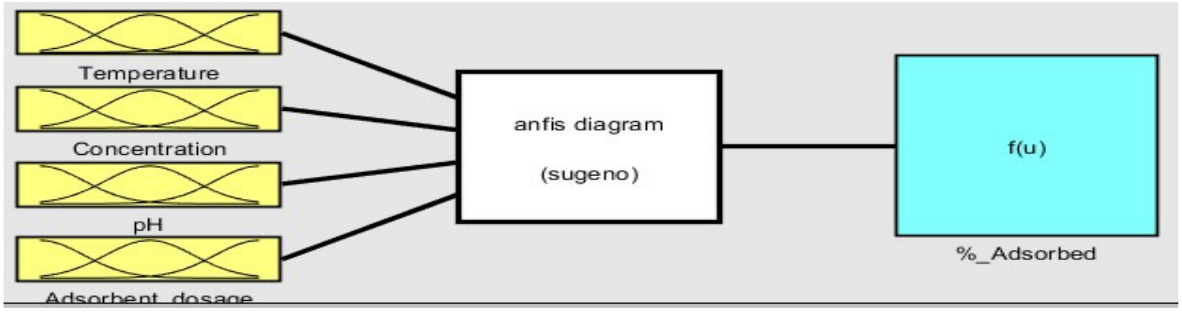

Figure 14: ANFIS Sugeno diagram of CR adsorption process

A 30x5 matrix (representing the input variables) and a 30x1 matrix (representing the output variable) were used in the MATLAB m-file. The Gaussian combination membership function (Guass2mf) was employed in checking the grid partition. Three membership functions were assigned to each input layer in generating the FIS. The ANFIS data was trained at 5 epoch iterations with an error tolerance of zero. A minimum error of 0.0402221 was produced after the 2nd epoch, which gives reliance on the adequacy of the ANFIS model in predicting the removal of CR dye. A plot of FIS against training data is shown in Figure 15. A hybrid-learning algorithm that makes use of the gradient method and the least squares method was used in optimizing the ANFIS model. A correlation coefficient of 0.9999 certifies the adequacy of the ANFIS model in predicting the removal of CR dye from wastewater using Umuahia clay.

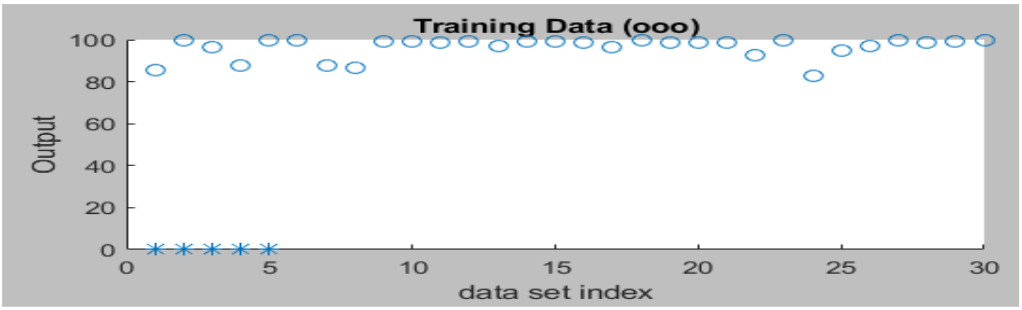

Figure 15: Plot of FIS against training data of CR adsorption

3.11. Comparison of Experimental Response with Predicted Response of RSM, ANN, and ANFIS Models

The result showed that the three models were good at modeling and predicting the removal of CR from wastewater in an adsorption process. ANFIS with the lowest residuals in most experimental data sets seems

to be the best at predicting the percentage of CR removed. Further statistical analyses were used to compare the adequacy of the three models in Table 8.

Table 7: Experimental and predicted results for CR removal

A:Temp °C	B:Conc mg/l	C:pH	D:Dosage g	Experimental response %	Models Predicted response		
					RSM	ANN	ANFIS
60	300	10	0.1	85.53	85.36	85.53	85.53
50	200	6	0.58	99.94	99.61	99.94	99.94
60	300	2	0.1	96.61	96.31	96.61	96.61
50	200	6	0.02	87.84	88.53	87.84	87.84
60	100	2	0.5	99.99	100.02	99.99	99.98
60	100	2	0.1	99.89	99.05	99.89	99.89
60	100	10	0.1	87.78	88.42	87.78	87.78
40	100	10	0.1	86.53	86.18	86.53	86.53
50	200	6	0.3	98.94	98.77	98.87	98.89
60	300	2	0.5	98.99	99.05	98.99	98.99
40	100	10	0.5	98.71	99.11	98.71	98.71
40	300	2	0.5	99.39	98.85	99.56	99.39
40	300	10	0.5	97.21	97.76	97.21	97.21
50	200	6	0.3	98.99	98.77	98.87	98.89
50	200	6	0.3	98.95	98.77	98.87	98.89
50	200	6	0.3	98.88	98.77	98.87	98.89
50	341.42	6	0.3	96.45	96.96	96.45	96.45
60	100	10	0.5	99.65	99.74	99.65	99.65
35.86	200	6	0.3	98.54	98.54	98.54	98.54
50	200	6	0.3	98.71	98.77	98.87	98.89
50	200	6	0.3	98.89	98.77	98.87	98.89
50	200	11.66	0.3	92.77	91.91	92.77	92.77
50	58.58	6	0.3	99.99	99.85	99.99	99.99
40	300	10	0.1	82.98	83.05	82.98	82.98
40	300	2	0.1	94.87	94.5	94.87	94.87
40	100	2	0.1	97.08	97.31	97.08	97.08
40	100	2	0.5	99.99	99.88	99.99	99.99
60	300	10	0.5	98.59	98.46	98.59	98.59
50	200	0.34	0.3	98.98	100.2	98.98	98.98
64.14	200	6	0.3	99.89	100.26	99.89	99.89

Table 8: Comparative statistical analysis of RSM, ANN, and ANFIS models

Model parameter	RSM	ANN	ANFIS
R^2	0.9500	0.99995	0.99999
APE	2.3×10^{-5}	-	6.3×10^{-6}
HYBRID	1.4×10^{-7}	2.5×10^{-7}	1.0×10^{-8}
RMSE	7.1×10^{-4}	9.2×10^{-4}	1.9×10^{-4}
SSE	4×10^{-4}	6.6×10^{-4}	3.0×10^{-5}

The model parameters investigated include R^2, APE, HYBRID, RMSE, and SSE. In the model indices, RSM showed the least modeling predictive ability using R^2 and APE, whereas APE could not fit in the ANN data. The ANN exhibited the least modeling predictive ability using HYBRID, RMSE, and SSE. ANFIS exhibited the best predictive ability when compared with the experimental data on CR dye removal from wastewater. Onu et al. (2021) reported similar results of the same trend on the removal of eriochrome black-T dye.

3.12. Comparative Performance of the Adsorbent

A comparison of the adsorption of Congo red dye with other adsorbents was made to ascertain the efficiency and relevancy of the modified clay used in this study. Maximum adsorption capacity (q_{max}), percentage removal, and adsorbent dosage were the parameters utilized in the comparison, as shown in Table 9. From Table 9, it can be seen that the adsorption capacity and removal efficiency of the modified Umuahia clay was higher than some of the reviewed adsorbents. The available of this clay in large deposit in Umuahia town, Nigeria with its adsorption efficiency makes it a viable effective and alternative adsorbent in the removal of Congo red dye from contaminated water. Table 10 presents the adsorption capacity and removal efficiency of the AUC in minimizing contaminant of dye industrial wastewater. The result shows a high reduction rate of the tested parameters after treatment, which thereby confirm AUC a reliable adsorbent for industrial wastewater treatment. The obtained result is in agreement with the previous report by Mustafa et al., (2023), who reported that Biosynthesis of Nickel Oxide Nanoparticles removes, 48.38% of EC, 49.24% of COD, and 67.05% of TDS from Azo Dye Industrial Wastewater.

Table 9: Comparison with other adsorbents

Adsorbent	Adsorbent dos (g)	Removal eff (%)	Ads capacity (mg/g)	Adsorbate	Reference
Pottery clay	0.05	94.75	1.086	Congo red	Baydaa and Lekaa, (2022)
Koura clay	0.05	82.95	0.224		
MgAl-LDH	0.05	60	769.23	Congo red	Mohamed et al., (2022)
PDFe/Al	1	99	411	Congo red	Khathutshelo et al., (2022)
Activate	0.02	80	11.9	Congo red	Hamd et al., (2023
Treated clay	0.3	90	39.80	Heavy metals	Paul and Mutsee, (2021)
Activated carbon	1	92.45	84.46	Congo red	Akande et al., (2023)
Agricultural waste (raw)	3.5	-	55.56	Congo red	Jegede et al., (2021)
(modified)	1.5	-	58.48		
Modified red clay	0.1	85	181.818	Methylene blue	Carazeanu et al., 2023
Banana stem	0.5	87	14.28	Remazole red	Kumar et al., (2022)
Rice bran	2	97.4	603	Crystal violet	Mojtaba et al., (2020)
Fe-bent	2	99	10.06	Arsenic(v)	Barakan et al., (2019)
Bentonite	1	95.21	151.5	Cr(III)	Amir et al., (2020)
	1	95.74	161.3	Cr(VI)	
Modified clay	0.5	97.5	98.74	Congo red	Present study

Table 10: Comparison of parameters of untreated and treated simulated industrial wastewater containing CR dye after 24hrs incubation

Parameters	Wastewater	Treated Wastewater	% Removal
EC (µs/cm)	101	17.4	83.17
TDS (mg/l)	51	3.8	92.55
COD (mg/l)	169	32	81.07
Color removal (mg/l)	100	0.0008	99.99

3.13. Regeneration of Adsorbent

The reusability capacity of the adsorbent was presented in Figure 16a-c. Figure 16a presents the effect of four different temperatures (303 k, 313 k, 323 k, and 333 k) on two different eluents (alkaline eluent and acidic eluent) after three desorption cycles. The result shows that CR dye desorption works perfectly with alkaline eluent due to the electrostatic repulsion that exits when the OH-ion of NaOH neutralizes the H^+ ion on the surface of the adsorbent. Additionally, the result also indicates that temperature did not have a significant effect during the process; therefore, low temperatures pose the benefit of cost efficiency. Figure 16b presents the effect of three eluent concentrations (1M, 3M, and 5M) on the desorption process.

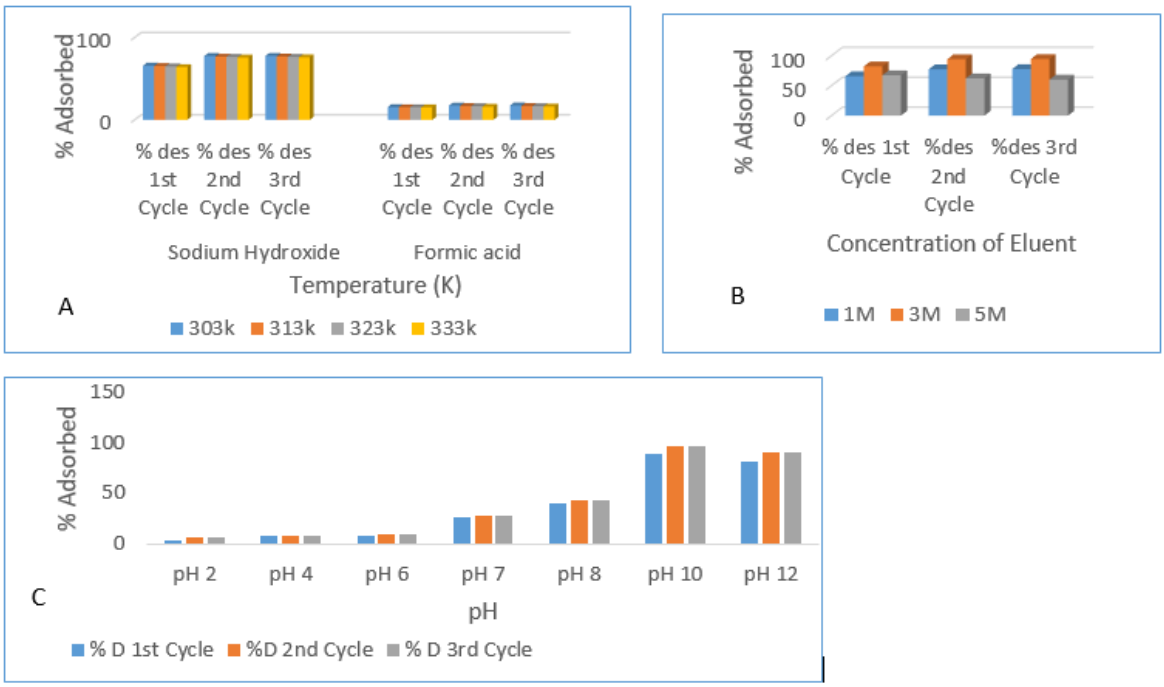

Figure 16: Effect of temperature, concentration, and pH of eluent on desorption of CR on AUC

The obtained result shows that low and higher concentrations did not favor the process, since 94.5% reusability capacity was recorded at 3M concentrations against 60.1% at 5M and 77.7% at 1M concentrations after three successive regeneration cycles. The slow rate of desorption at 1M is attributed to a weak driving force and thus requires a larger volume of eluent to achieve the same objective as with mid-concentrated eluent, whereas the low desorption rate at higher concentrations is due to the adverse effect of eluent high concentration strength, which may destabilize or weaken the chemical and pore structure of the adsorbent. Figure 16c presents the effect of different pHs of the eluent (pH 2-12) on the desorption process. The highest reusability capacity of 97.2 was achieved at pH 10 after three successive regeneration cycles. This high reusability capacity at pH 10 instead of pH 12 is attributed to high alkalinity strength, which may weaken both the chemical and pore structures of the adsorbent surface and thereby lead to poor outcomes. This outcome validates the results of choice and concentration of eluent, which favor alkaline eluent and 3M concentration, respectively. Finally, Figure 10 shows an insignificant change in reusability capacity after the 2^{nd} and 3^{rd} desorption cycles, irrespective of whether the 3^{rd} was the best. The minor change in reusability capacity is attributed to characteristics of equilibrium. The obtained result is in agreement with the previous report by Zhang et al., (2018), who reported that temperature has an insignificant effect on the desorption of the five synthetic azo dyes (tartrazine, amaranth, carmine, sunset yellow, and allura red). They also reported that optimized desorption efficiency was achieved at pH 9. Wang et al., (2020) reported similar results with

the same trend on effect concentration. Himanshu, (2021) reported that alkali eluents are best used for anionic adsorbates.

4. CONCLUSION

The present study established the potential of AUC as an adsorbent for the removal of dye from an aqueous solution. The adsorption of CR onto AUC was found to be dependent on the pH solution, initial dye concentration, temperature, adsorbent dosage, contact time, and adsorbent particle size. The equilibrium adsorption data was best represented by the Vieth-Sladek model, while D-R yields the highest maximum adsorption capacity (q_m) value of 140.53 mg g^{-1}. The adsorption kinetic data was best described by pseudo-nth-order kinetic models. From the thermodynamic studies, the adsorption process was spontaneous, endothermic, favorable, and physical, and this was in agreement with the findings of the equilibrium adsorption parameters. The ANN, ANFIS, and RSM models were adequate for predictive modeling of the adsorption process, though the statistical analysis indicated that the ANFIS model was marginally better than the ANN and RSM.

6. CONFLICT OF INTEREST

There is no conflict of interest associated with this work.

REFERENCES

Adebayo M.A, Jabar J.M, Amoko J.S, Openiyi E.O, and Shodiya O.O. (2022). Coconut husk-raw clay-Fe composite: preparation, characteristics and mechanisms of Congo red adsorption. *Sci Rep*. 2022 Aug 23;12(1):14370. doi: 10.1038/s41598-022-18763-y.

Akande, J.A, Adeogun A.I, Uzosike A.S. (2023). Removal of Congo Red Dye from Simulated Wastewater Using Activated Carbon Derived from Corn Cobs; Kinetics and Equilibrium Studies, *Global Journal of Pure and Applied Chemistry Research*, Vol.11, No.1, pp.1-19

Amini A, Younesi H, Bahramifar N, Lorestani A,Ghorbani F, Daneshi A and Sharifzadeh M. (2008). Application of Response Surface Methodology for Optimization of Lead Biosorption in an Aqueous Solution by Aspergillusniger. *J. Hazard. Mater*, 154, 694-702.

Amir A, Rauf F, Hossein E, and Sajad T. (2020). The role of bentonite clay and bentonite clay@MnFe2O4 composite and their physico-chemical properties on the removal of Cr(III) and Cr(VI) from aqueous media. *Environ Sci Pollut Res* https://doi.org/10.1007/s11356-020-07756-x

Arana J.M.R.R., and Mazzoco R.R. (2010). Adsorption studies of methylene blue and phenol onto black stone cherries prepared by chemical activation, *J. Hazard. Mater*. 180 (2010) 656–661. Doi:10.1016/j.jhazmat.2010.04.086.

Arulkumar, M., Sathishkumar, P., Palvannan, T. (2011). Optimization of orange G dye adsorption by activated carbon of thespesiapopulnea pods using response surface methodology. *Journal of Hazardous Materials*. 186 (1), 827–834. https://doi.org/10.1016/j.jhazmat.2010.11.067.

Bahman N and Sina F.A. (2018). Application of ANFIS, ANN, and logistic methods in estimating biogas production from spent mushroom compost (SMC). *Resources, Conservation & Recycling* 133 169–178 https://doi.org/10.1016/j.resconrec.2018.02.025.

Barakan S, Aghazadeh V, Samiee B. A, Mohammadi S. (2019). Thermodynamic, kinetic and equilibrium isotherm studies of As(V) adsorption by Fe(III)-impregnated bentonite. *Environ Dev Sustain*. https://doi.org/10.1007/s10668-019-00424-2

Baydaa N. A, and Lekaa H. K. (2022). Removal of Congo Red Dye from Aqueous Solution Using Different Clays Adsorbent. *Journal of Algebraic Statistics* Volume 13, No. 3, 2022, p. 861 - 875 https://publishoa.com ISSN: 1309-3452 861

Bhattacharyya K.G., and Sharma A. (2005). Kinetics and thermodynamics of methylene blue adsorption on Neem (Azadirachta indica) leaf powder, *Dyes Pigments* 65 51–59. Doi:10.1016/j.dyepig2004.06.016

Cáceres-Jensen L., Rodríguez-Becerra J., Parra-Rivero J., Escudey M., Barrientos L, and Castro-Castillo V. (2013). Sorption kinetics of diuron on volcanic ash derived soils. *Journal of Hazardous Materials*. 2013;261: 602–613. doi: 10.1016/j.jhazmat.2013.07.073.

Carazeanu P.I., Roscaa. I, and Dumbravaa. A. (2023). Modified red clays as adsorbents in the removal of cationic dyes from aqueous solutions. *Digest Journal of Nanomaterials and Biostructures* Vol. 18, No. 2, April - June 2023, p. 567 – 578

Cheung, W. H., Szeto, Y. S.; and Mckay, G. (2007). Intraparticle diffusion processes during acid dye adsorption onto chitosan. *Bioresour.Technol*. 98(15), 2897-2904. Doi.org/10.1016/j.biortech.2006.09.045

Dal S. K, and Meenal G. (2022). Treatment of Textile Dyeing Effluent Using Agriculture Waste Based Adsorbents - A Review. *Chemical Science International Journal.* Volume 32 [Issue 6] DOI: 10.9734/CSJI/2023/v32i6870

Dalia, K. M; Mohamad, A. M. S; Wan, A. W. A. K; Azni, I, and Zurina, Z. A. (2011). Batch adsorption of basic dye using acid treated kenaffibre char: equilibrium, kinetic and thermodynamics studies. *Chem Eng. J.* 181-182, 449-457. Doi: 10.1016/j.cej.2011.11.116.

Doˇgan M, Abak H, and Alkan M. (2009). Adsorption of methylene blue onto hazelnut shell: kinetics, mechanism and activation parameters. *J. Hazard. Mater.* 164, 172–181. Doi.org/10.1016/j.jhazmat.2008.07.155

Dotto, G. L., and Pinto, L. A. A. (2011). Adsorption of Food Dye Acid Blue 9 and Food Yellow 3 onto Chitosan: stirring Rate effect in Kinetics and Mechanism. *J Hazard.Mater*. 187, 164-170.

Dubinin M.M and Radushkevich L.V. (1947). Equation of the characteristic curve of activated charcoal. *Proc Acad Sci Phys Chem* Sect USSR 55:331–333

El-Halwany M.M. (2010). Study of adsorption isotherms and kinetic models for methylene blue adsorption on activated carbon developed from Egyptian rice hull (Part II), *Desalination* 250(1) 208–213. Doi.org/10.1016/j.desal.2008.07.030.

Freundlich H.M.F. (1906). Over the adsorption in solution *J. Phys. Chem.* 57, 385-470.

Gonzalez C.R.T., Subathra M.S.P., and Manoj K.N. (2020). Modelling the daily reference evapotranspiration in semi-arid region of South India: A case study comparing ANFIS and empirical models. *Information Processing in Agriculture* 2-12. https://doi.org/10.1016/j.inpa.2020.02.003.

Hamd A, Salah D, Alyafei H. F, Soliman N. K, El-Reedy A. A. M, Elzanaty A. M, Al-Saeedi S. I, Al-Ghamdi A, Shaban M, and El-Sayed R. (2023). NaOH-Activated Natural Glauconite for Low-Cost Adsorption of Congo Red Dye *Water* 2023, 15, 3753. https://doi.org/ 10.3390/w15213753

Hameed, B. H. and Hakimi, H. (2008). Utilization of durian (DurioZibethinus Murray) peel as low cost sorbent for the removal of acid dye from aqueous solutions. *Biochem.Eng.J.* 39(2), 338-343. Doi:10.1016/j.bej.2007.10.005

Himanshu P. (2021). Review on solvent desorption study from exhausted adsorbent. *Journal of Saudi Chemical Society* (2021) 25, 101302

Hu, Z; Chen, H; ji, F, and Yuan, S. (2010). Removal of Congo red from aqueous solution by cattail root, *j. Hazard. Mater.* 173(1-3). 292-297. Doi.org/10.1016/j.jhazmat.2009.08.082.

Iheanacho C. O., Nwabanne J.T. and Onu C.E. (2019). Optimum Process Parameters for Activated Carbon Production from Rice Husk for Phenol Adsorption. Current Journal of *Applied Science and Technology,* 36(6): 1-11. https://doi.org/10.9734/CJAST/2019/v36i630264

Imessaoudene, A.; Cheikh, S.; Hadadi, A.; Hamri, N.; Bollinger, J.-C.; Amrane, A.; Tahraoui, H.; Manseri, A.; Mouni, L. (2023). Adsorption Performance of Zeolite for the Removal of Congo Red Dye: Factorial Design Experiments, Kinetic, and Equilibrium Studies. *Separations* 2023, 10, 57. https://doi.org/10.3390/separations10010057

Ismat A. E, Marufa K, Most. Afroza K, Owaleur R.M.d., Anis-Ul-Haque K. M., and

Jegede M. M., Durowoju O. S., and Edokpayi J. N. (2021). Sequestration of Hazardous Dyes from Aqueous Solution Using Raw and Modified Agricultural Waste. *Adsorption Science & Technology*, Volume 2021, Article ID 6297451 https://doi.org/10.1155/2021/6297451

Jovanovic, D.S. (1969). Physical adsorption of gases—II: Practical application of derived isotherms for monolayer and multilayer adsorption. *Kollozd Z.*, 235, 1214–1225.

Juraj B. (2023). Controversial Issues Related to Dye Adsorption on Clay Minerals: A Critical Review. *Molecules* 2023, *28*(19), 6951; https://doi.org/10.3390/molecules28196951

Kausar A., Bhatti H. and Mackinnom G. (2013). Equilibrium kinetic and thermodynamics studies on the removal of U (VI) by low-cost agricultural waste, *Colloids and Surface B*, Vol 111, 2013, 124-133. Doi.org/10.1016/j.colsurfb.2013.05.025.

Khathutshelo L. M., Vhahangwele M., Johannes P. M., Nils H., and Hendrik G. B. (2022). Nanotechnology in the Restoration of Polluted Soil. *Nanomaterials (Basel).* 12(5): 776. doi: 10.3390/nano12050776.

Kumar K. A, Bharath M, and Krishna B. M. (2022). Adsorption kinetics of reactive dye using agricultural waste: banana stem. *Water Practice and Technology* 17 (1): 128–138. https://doi.org/10.2166/wpt.2021.106

Ladhe, U. V., Wankhede, S. K., Patil, V. T., and Patil, P. R. (2011). Adsorption of Eriochrome Black-T from Aqueous Solution on Activated Carbon prepared from Mosambi Peel. *Jol.of Applied Sci. in Environmental Sanitation*, 6(2), 149-154.

Lafi R, Montasser I, and Hafiane A. (2019). Adsorption of Congo red dye from aqueous solutions by prepared activated carbon with oxygen-containing functional groups and its regeneration. *Adsorpt. Sci. Technol.* 2019;**37**:160–181. doi: 10.1177/0263617418819227.

Langmuir I. (1916). The constitution and fundamental properties of solids and liquids. *J. AM. Chem. Soc.* 38(11), 2221-2295. Doi.org/10.1021/ja02268a022.

Lata H., Garg V., and Gupta R. (2007). Removal of basic dye from aqueous solution by adsorption using Partheniumhysterophorus: an agricultural waste, *Dye pigments* 74(3), 653-658 .doi.org/10.1016/j.dye.2006.04.007.

Mahammedi F and Benguella B., (2016). Adsorption of methylene blue from aqueous solutions using natural clay. *J. Mater. Environ. Sci. 7 (1) (2016) 285-292*

Mahmoodi M., Hayati M. B., Arami M., and Lan C. (2011). Adsorption of textile dyes on Pine Cone from colored wastewater: Kinetic, equilibrium and thermodynamic studies. *Desalination* 268(1-3), 117-125. Doi: 10.1016/j.desal.2010.10.007.

Mahmoud El O., Mohamed L., Hicham A. O., Younes B., Abdelhadi A., Abdelaziz E., Abdelaziz A. A., and Abdellatif L. (2019). Efficient removal of p-nitrophenol from water using montmorillonite clay: insights into the adsorption mechanism, process optimization, and regeneration. *Environ Sci Pollut Res* 26:19615–19631. https://doi.org/10.1007/s11356-019-05219-6

Manpreet S.B., DhritiKapoor, R.K., Kalia, A. S. R., and Ashwani K.T. (2011). RSM and ANN modeling for electrocoagulation of copper from simulated wastewater: Multi objective optimization using genetic algorithm approach. Desalination 274 (2011) 74–80. doi: 10.1016/j.desal.2011.01.083.

Mingyi, F., Tongjun, L., Jiwei, H., Rensheng, C., Xionghui, W., Xuedan, S., and Wenqian, R. (2017). Artificial neural network modeling and genetic algorithm optimization for cadmium removal from aqueous solutions by reduced graphene oxide-supported nanoscale zero-valent iron (nzvi/rgo) composites. *Materials.* 10 (544), 1 – 22. doi:10.3390/ma10050544.

Mohamed A. F., Abdelfattah M. S., Hanem F. K., Noha B, Walaa A., Khadijah H. A., and Ibrahim T. R. (2022). Optimized adsorption and effective disposal of Congo red dye from wastewater: Hydrothermal fabrication of MgAl-LDH nanohydrotalcite-like materials *Arabian Journal of Chemistry* Volume 15, Issue 11, November 2022, 104171. https://doi.org/10.1016/j.arabjc.2022.104171

Mohammed B., Mustapha D., and Ftiha D. (2022). Adsorption of dye using natural clay from water. *Journal of Environmental Engineering and Science.* Volume 17 Issue 4, December 2022, pp.175-183. https://doi.org/10.1680/jenes.21.00051

Mohammed G. H., Magdy A. W., Hosni A. G., and Ahmed S. E. (2023). Adsorption of Rose Bengal dye from waste water onto modified biomass. *Sci Rep.* 2023; 13: 14776. doi: 10.1038/s41598-023-41747-5

Mojtaba R., Majid B., Naser M., and Mohammad A. A. (2020). Adsorption of crystal violet dye by agricultural rice bran waste: Isotherms, kinetics, modeling and influencing factors. *Environmental Engineering Research* 2021;26(3): 200128. DOI: https://doi.org/10.4491/eer.2020.128

Mourabet, M.E., Rhilassi, A., Bennani-Ziatni, M., and Taitai, A. (2014). Comparative Study of artificial neural network and response surface methodology for modelling and optimization the adsorption capacity of fluoride onto apatitictri calcium phosphate. *Universal Journal of Applied Mathematics*. 2(2), 84-91. doi: 10.13189/ujam.2014.020202

Muhammed O, and Çiğdem S. Ö. (2022). Equilibrium Studies for Dye Adsorption onto Red Clay. *Journal of Engineering and Natural Sciences* 3:2 (2022) 36-45. https://dergipark.org.tr/tr/pub/naturengs DOI: 10.46572/naturengs.1120218

Mustafa S, Mahmood F, Shafqat U, Hussain S, Shahid; Batool F, Elnour R. O, Hashem M, Asseri T. A. Y, and Shahzad T. (2023). The Biosynthesis of Nickel Oxide Nanoparticles: An Eco-Friendly Approach for Azo Dye

Decolorization and Industrial Wastewater Treatment. *Sustainability* 2023, 15, 14965. https://doi.org/10.3390/su152014965

Nayoon C, Yeongkyun S, Tae-Hyun K, Yuri P, and Yuhoon H. (2022). Adsorption behaviors of modified clays prepared with structurally different surfactants for anionic dyes removal. *Environmental Engineering Research* 2023; 28(2): 210076. DOI: https://doi.org/10.4491/eer.2022.076

Oguanobi N. C., Onu, C. E., and Onukwuli O. D. (2019). Adsorption of a dye (Crystal Violet) on acid modified non-conventional adsorbent. *Journal of Chemical Technology and Metallurgy*, 54 (1) 95-110.

Oguanobi N.C, Okonkwo G, Onukwuli O.D, Ude C.N, Anike E.N. (2024b). Kinetic and Modeling of Anionic Dye Adsorption onto Acid modified Ihiala Clays: ANN, ANFIS and RSM comparative analysis. *UNIZIK Journal of Engineering and Applied Sciences* 3(2), June (2024), 608-613. Accepted. Journal homepage: https://journals.unizik.edu.ng/index.php/ujeas

Oguanobi N.C, Ude C.N, Nnaji P.C, Onukwuli O.D, Anike E.N. Okonkwo G, and Okonkwo C.H. (2024a). Adsorption Behaviors of Raw Clay for Cationic Dyes Removal: Equilibrium, Kinetic Modeling, Thermodynamics, and RSM Optimization, *Umudike Journal of Engineering and Technology.* vol. 10 No. 1, June 2024. Doi: https://doi.org/10.33922/j.ujet_v10i1_19.

Onu C. E, Nwabanne J. T., Ohale P. E, and Asadu C. O. (2021). Application of ANN and RSM Techniques in Optimal Parameter Evaluation for Turbidity Removal from Abattoir Effluent using Valorized Chicken Bone Coagulant South *African Journal of Chemical Engineering* 36 (2021) 24–42. https://doi.org/10.1016/j.sajce.2020.12.003

Onu C. E., Oguanobi N. C., Okonkwo C. O., and Nnamdi-Bejie J. (2020). Application of Modified Agricultural Waste in the Adsorption of Bromocresol Green Dye. *Asian Journal of Chemical Sciences.* 7(1): 15-24. https://doi.org/10.9734/AJOCS/2020/v7i119011

Onu, C.E. and Nwabanne, J.T. (2014). "Application of Response Surface Methodology in Malachite green adsorption using Nteje clay". *Open Journal of Chemical Engineering and Science.* 1 (2) 19 – 33.

Paul E. D, and Mutsee T. (2021). Treated Clay Mineral as Adsorbent for the Removal of Heavy Metals from Aqueous Solution *Applied science and engineering progress* Vol 14, No 3 https://doi.org/10.14416/j.asep.2021.04.002

Popoola, T. J., Okoronkwo, A. E., Oluwasina, O. O., and Adebayo, M. A. (2021). Preparation, characterization, and application of a homemade graphene for the removal of Congo red from aqueous solutions. *Environ. Sci. Poll. Res.* 28, 52174–52187.

Reddy S.M.C., Sivaramakrishna L., and Reddy V.A. (2011). The use of an agricultural waste material, jujba seeds for the removal of anionic dye (Congo red) from aqueous medium. *Journal of Hazardous Materials* 203-204 (012) 118-127.

Redlich O, Peterson D.L. (1959). A useful adsorption isotherm. *Journal of Physical Chemistry.* 1959;63:1024.

Sabarish R, Jasila K, Aswathy J, Jyotishkumar P, Jaewoo L, Jyothi Mannekote S, Rajarathinam N, and Suchart S, (2022). Adsorption of anionic dye onto ZSM-5 zeolite-based bio membrane: Characterizations, kinetics and adsorption isotherm. *Journal of polymers and the environment*. https://doi.org/10.21203/rs.3.rs-1191111/v1

Salleh, M. A. M., Mahmoud, D. K., Karim, W. A., and Idris, A. (2011). Cationic and anionic dye adsorption by agricultural solid waste: a comparative review. *Desalination* 280 (1-3), 1-13.

Singha B. and Das S. (2013). Adsorptive removal of Cu (II) from aqueous solution and industrial effluent using natural and agricultural waste. *Colloids and surface* B, Vol 107, 2013, 77-106. Doi.org/10.1016/j.colsurfb.2013.01.060.

Srivastava, V. C., Mall, I. D., and Mishra, M. (2007). Adsorption thermodynamics and isosteric heat of adsorption of toxic metal ion onto bagasse fly ash (BFA) and rice husk ash (RHA), *Chem. Eng. J.*132, 267-278.

Venkatesh P.M., and Karthikeyan R. (2018). Comparative studies on modelling and optimization of hydrodynamic parameters on inverse fluidized bed reactor using ANN-GA and RSM. *Alexandria Engineering Journal* 57:3019–3032. https://doi.org/10.1016/j.aej.2018.05.002.

Vieth W.R, and Sladek K.J. (1965). A model for diffusion in a glassy polymer. *J Colloid Sci* 20:1014–1033. Doi 10.1016/0095-8522(65)90071-1.

Wang G., He D., Fengchun Z.F., Hu J., Lee Y., Shi J., and Xu J. (2020). Extraction and purification of ustiloxin A from rice false smut balls by a combination of macroporous resin and high-speed countercurrent chromatography. *Food Production, Processing and Nutrition* 2:29 https://doi.org/10.1186/s43014-020-00043-9

Weber, W.J., and Morris, J.C. (1963). Kinetics of Adsorption on carbon from solutions. *Journal of the sanitary Engineering Division*, 89, 31-39.

Wu X., Hui K. N., Lee S. K., Zhou W., Chen R., Hwang D. H., Cho Y. R., and Son Y. G. (2012). Adsorption of basic yellow 87 from aqueous solution onto two different mesoporous adsorbents. *Chemical Engineering Journal* 180,91-98. doi:10.1016/j.cej.2011.11.009

Wu, C. H. (2007). Adsorption of reactive dye onto carbon nanotubes: equilibrium, kinetics and thermodynamics. *J. Hazard mater.* 144(1-2). 93-100. Doi:10.1016/j.jhazmat.2006.09.083.

Zhang X., Zhang J., Li W., Yang Y., Qin P., Zhang X., and Lu M. (2018). Magnetic graphene oxide nanocomposites as the adsorbent for extraction and pre-concentration of azo dyes in different food samples followed by high-performance liquid chromatography analysis. *Taylor & Francis Group* https://doi.org/10.1080/19440049.2018.1526415

Zhi L., Xiaohai H., Yi M., Bing G., Yiling S., Jianghui Z., Soon H. T. (2022). Eggplant biomass based porous carbon for fast and efficient dye adsorption from wastewater. *Industrial Crops and Products*.Volume 187, Part B, 1 November 2022, 115510 https://doi.org/10.1016/j.indcrop.2022.115510Get rights and content

Zineb El K., Jaouad B., Nouhaila F., Abdelali El M., Avni B., Zaki S., Hanae O., Farid K., Musaab D., Hiba-Allah N., Abdel-Rhman Z. G., Mohammed B., Amar H., and Nouredine EL M. (2023). Physicochemical Characterization of Clay and Study of Cationic Methylene Blue Dye Adsorption. *ACS Omega* 2023, 8, 43, 40848–40863. https://doi.org/10.1021/acsomega.3c06019.